Role of cardiac ryanodine receptor calmodulin-binding domains in mediating the action of arrhythmogenic calmodulin N-domain mutation N54I

Søndergaard, Mads T; Liu, Yingjie; Guo, Wenting; Wei, Jinhong; Wang, Ruiwu; Brohus, Malene; Overgaard, Michael T; Chen, S R Wayne

Published in:
The FEBS Journal

DOI (link to publication from Publisher):
10.1111/febs.15147

Publication date:
2020

Document Version
Accepted author manuscript, peer reviewed version

MR. MADS TOFT SØNDERGAARD (Orcid ID : 0000-0001-6779-5109)
PROF. MICHAEL TOFT OVERGAARD (Orcid ID : 0000-0002-1423-2481)

Received Date : 21-Dec-2018
Revised Date : 12-Sep-2019
Accepted Date : 19-Nov-2019

Role of cardiac ryanodine receptor calmodulin-binding domains in mediating the action of arrhythmogenic calmodulin N-domain mutation N54I

Mads T. Søndergaard[a,b*], Yingjie Liu[b], Wenting Guo[b], Jinhong Wei[b], Ruiwu Wang[b], Malene Brohus[a], Michael T. Overgaard[a] and S.R. Wayne Chen[b*]

From the [a]Department of Chemistry and Bioscience, Aalborg University, 9220 Aalborg, Denmark; and the [b]Libin Cardiovascular Institute of Alberta, Department of Physiology and Pharmacology and Department of Biochemistry and Molecular Biology, University of Calgary, Calgary, Alberta, T2N 1N4, Canada

[*]To whom correspondence should be addressed: Department of Chemistry and Bioscience, Aalborg University, 9220 Aalborg, Denmark. Tel.: 40616849; mts@bio.aau.dk or the Libin Cardiovascular Institute of Alberta, Department of Physiology and Pharmacology, HRIC GAC58, 3330 Hospital Dr. N.W., Calgary, AB, Canada. Tel.: 403-220-4235; Fax: 403-270-0313; swchen@ucalgary.ca

Running Title

Role of RyR2 CaMBDs in the action of CaM-N54I

Keywords

Arrhythmia, calmodulin, ryanodine receptor, intracellular Ca^{2+} signalling, ion channel regulation

Abbreviations

calmodulin (CaM), CaM-binding domain (CaMBD), sarcoplasmic reticulum (SR), cardiac SR Ca^{2+} release channel or ryanodine receptor type 2 (RyR2), voltage-gated Ca^{2+} channels ($Ca_V1.2$), cytosolic free Ca^{2+} ($[Ca^{2+}]_{cyt}$), catecholaminergic polymorphic ventricular tachycardia (CPVT), store-overload induced Ca^{2+} release (SOICR), free Ca^{2+} concentration ($[Ca^{2+}]_{free}$), tritium ($[^3H]$), the CaM target database (CTD), dissociation constant (K_D), ryanodine association rate (K), total ryanodine binding at near equilibrium (B_{eq}), pH- and Ca^{2+}-buffered solutions (pCa-buffer), glycol-bis(2-aminoethylether)-tetraacetic acid (EGTA), nitrilotriacetic acid (NTA), Gibb's free energy of binding ($\Delta\Delta G^o$), endoplasmic reticulum (ER), intracellular-like medium (ICM)

human RyR type 1-3 (hRyR1-3), mouse RyR2 (mRyR2), ratio of yellow to cyan D1ER protein fluorescence (YFP/CFP), SR/ER Ca^{2+} ATPase 2 (SERCA2b), control (Ctrl), peptidyl-prolyl cis-trans isomerase FKBP1B (FKBP12.6), cryogenic electron microscopy (cryo-EM), sample standard deviation (SD), fluorescence resonance energy transfer (FRET), confidence interval (CI), ratio of yellow to cyan D1ER protein fluorescence (YFP/CFP), normalized Fluo-3 fluorescence ($\Delta F/F_0$).

ABSTRACT

The Ca^{2+}-sensing protein calmodulin (CaM) inhibits cardiac ryanodine receptor (RyR2)-mediated Ca^{2+} release. CaM mutations associated with arrhythmias and sudden cardiac death have been shown to diminish CaM-dependent inhibition of RyR2, but the underlying mechanisms are not well understood. Nearly all arrhythmogenic CaM mutations identified are located in the C-domain of CaM and exert marked effects on Ca^{2+} binding to CaM and on the CaM C-domain interaction with the CaM-binding domain 2 (CaMBD2) in RyR2. Interestingly, the arrhythmogenic N-domain mutation CaM-N54I has little or no effect on Ca^{2+} binding to CaM or the CaM C-domain-RyR2 CaMBD2 interaction, unlike all CaM C-domain mutations. This suggests that CaM-N54I may diminish CaM-dependent RyR2 inhibition by affecting CaM N-domain interactions with RyR2 CaMBDs other than CaMBD2. To explore this possibility, we assessed the effects of deleting each of the four known CaMBDs in RyR2 (CaMBD1a, -1b, -2 or -3) on the CaM-dependent inhibition of RyR2-mediated Ca^{2+} release in HEK293 cells. We found that removing CaMBD1a, CaMBD1b, or CaMBD3 did not alter the effects of CaM-N54I or CaM-WT on RyR2 inhibition. On the other hand, deleting RyR2-CaMBD2 abolished the effects of both CaM-N54I and CaM-WT. Our results support that CaM-N54I causes aberrant RyR2 regulation via an uncharacterised CaMBD or less likely CaMBD2, and that RyR2 CaMBD2 is required for the actions of both N- and C-domain CaM mutations. Moreover, our results show that CaMBD1a is central to RyR2 regulation, but CaMBD1a, CaMBD1b and CaMBD3 are not required for CaM-dependent inhibition of RyR2 in HEK293 cells.

INTRODUCTION

The cardiac sarcoplasmic reticulum (SR) Ca^{2+} release channel (or ryanodine receptor type 2, RyR2) controls the intracellular release of Ca^{2+} stored in the SR in cardiomyocytes [1]. During cardiac excitation, a small influx of extracellular Ca^{2+} into the cytoplasm through voltage-gated Ca^{2+} channels ($Ca_V1.2$) activates RyR2 channels, embedded in the SR membrane, to release intracellularly stored Ca^{2+}. This intracellular Ca^{2+} release increases the cytosolic free Ca^{2+} ($[Ca^{2+}]_{cyt}$) throughout the cardiomyocyte, and binding of Ca^{2+} to the myofilaments results in contraction. Ca^{2+} re-uptake to the SR and extrusion to the extracellular space then returns the cardiomyocyte to resting intracellular Ca^{2+} conditions [1,2]. Proper cardiac function requires intricate control of the Ca^{2+} release-uptake cycle, and therefore RyR2 activity is regulated by numerous proteins and signaling molecules, including the cytoplasmic Ca^{2+}-sensing protein calmodulin (CaM) [1-5]. CaM has two Ca^{2+} binding domains (N- and C-domain) that each contains two Ca^{2+}-binding EF-hand motifs, and CaM binds stoichiometrically to the homotetrameric RyR2 Ca^{2+} release channels (Figure 1).

CaM generally inhibits RyR2 Ca^{2+} release both at diastolic and systolic $[Ca^{2+}]_{cyt}$, and the tripartite interaction between the CaM C-domain, Ca^{2+} and the central CaM-binding domain (CaMBD2) in RyR2 is pivotal for CaM's inhibition of RyR2 Ca^{2+} release, however both the N- and C-domain of CaM are required for adequate RyR2 regulation [1,4-14]. The two CaM domains have distinct affinities and kinetics for Ca^{2+} binding, and may therefore separately interact with different regions of RyR2 in a $[Ca^{2+}]_{cyt}$-dependent manner, but whether CaM's inhibition of RyR2 involves more than one RyR2 region remains unclear [4-10,15,16]. Recent studies have coalesced the potential RyR2 regions to four CaMBDs, here referred to as CaMBD1a, -1b, -2 and -3 (Figure 2 and Table 1), but CaMBD2 is the only bona-fide RyR2 CaMBD functionally characterized and validated [6-9,12-14,17]. The CaM C-domain binding to CaMBD2 around RyR2 Trp-3587 is a prerequisite for CaM-dependent RyR2 inhibition. However, the CaM N-domain can also bind CaMBD2 around Phe-3603, albeit the function of the latter interaction is undefined [6-9,15-19]. On the other hand, the functional significance of CaMBD1a, -1b or -3 for CaM-dependent RyR2 inhibition remains unknown [5,15,20]. It has been proposed that the CaM N-domain shifts between RyR2 binding sites in response to changes in $[Ca^{2+}]_{cyt}$ during cardiomyocyte Ca^{2+} oscillations, and that RyR2 CaMBDs other than CaMBD2 may be involved in this process [1,4-13,15,16,21]. Recent cryogenic electron microscopy (cryo-EM) structures of the RyR2-CaM complexes support that the CaM N-domain shifts with increasing Ca^{2+}, but not to CaMBD1a, -1b or -3. However, Gong et al. and other studies also demonstrate that RyR2-CaM conformations are numerous and depend on the ligands present in the channel complex [5,17,22-24].

Mutations in CaM cause severe forms of cardiac arrhythmia, most likely due to perturbation of the intricate Ca^{2+} signals required for regulating cardiac excitation and contraction. Of the 15 CaM mutations

currently known, 14 are in the CaM C-domain and can cause insufficient RyR2 inhibition, most likely due to aberrant interactions among the CaM C-domain, Ca^{2+} and RyR2 CaMBD2 [8,16,25-37]. However, one CaM mutation is located in the N-domain, N54I, and specifically causes catecholaminergic polymorphic ventricular tachycardia (CPVT) highly likely due to its diminished inhibition of RyR2. Indeed, CaM-N54I causes excessive RyR2 activity in HEK293 cells, isolated cardiomyocytes and of single RyR2 channels, yet CaM-N54I binds to Ca^{2+}, a RyR2 CaMBD2 peptide, and intact RyR2 channels almost indistinguishably from the CaM-WT [8,16,25,27,37-40]. These observations raise an interesting question of whether the CaM N-domain interacts with other RyR2 CaMBDs, such as CaMBD1a, -1b or -3, rather than CaMBD2, and that the N54I mutation impairs RyR2 inhibition by perturbing such interactions.

In this study, we investigated whether the effects of CaM-N54I on CaM-dependent RyR2 inhibition are dependent on RyR2 CaMBD1a, -1b, -2 or -3. Usefully, this also involved investigating the role of the putative CaMBD1a, -1b and -3 with respect to native CaM-dependent regulation of RyR2. To this end, we individually removed each of the CaMBDs in RyR2 and determined their effects on CaM-dependent inhibition of RyR2-mediated Ca^{2+} release in HEK293 cells, both during store-overload induced Ca^{2+} release (SOICR) in intact cells, and in permeabilized cells with a sustained free Ca^{2+} concentration ($[Ca^{2+}]_{free}$) of 1 μM [7,8,16,41]. We evaluated CaM-dependent RyR2 inhibition by CaM-WT and CaM-N54I. CaM-WT inhibited RyR2 Ca^{2+} release in intact cells despite deleting either CaMBD1a, -1b or -3, while CaM-N54I decreased CaM-dependent RyR2 inhibition, compared to CaM-WT. Using permeabilized cells in the presence of 1 μM cytosolic $[Ca^{2+}]_{free}$, exogenously added CaM-WT markedly inhibited RyR2 Ca^{2+} release despite deletion of CaMBD1a, -1b and -3, and again CaM-N54I was less effective in inhibiting RyR2 than the CaM-WT. In comparison, deleting CaMBD2 ablated the effect of CaM-WT or CaM-N54I on RyR2 inhibition in either assay. We also found that CaM-WT inhibited ryanodine binding to RyR2 despite deleting CaMBD1b or -3, and that CaM-N54I in comparison failed to inhibit ryanodine binding, regardless of CaMBD deletions. Taken together, we found that CaMBD1a is integral to native RyR2 regulation, but only CaMBD2, and not CaMBD1a, -1b or -3, is strictly required for CaM-dependent inhibition of RyR2 Ca^{2+} release under our experimental conditions. Our results support the notion that while CaM-N54I requires RyR2 CaMBD2 for its effect, the N54I mutation decreases the inhibition of RyR2 via an additional CaMBD that has yet to be identified.

RESULTS

Three-dimensional localizations of known and proposed RyR CaM binding domains (CaMBDs)

To structurally evaluate the positions of the RyR2 CaMBDs in the homotetrameric channel, we used the recently available cryo-EM structures of RyR2 in complex with CaM in the absence and presence of Ca^{2+}

(Figure 1 and Table 1) [17]. Gong et al. show that in the absence of Ca^{2+} the CaM N-domain binds RyR2 in a cleft formed by the handle, helical, and central domains (Figure 1A and -C), although not via the CaM N-domain's Met rich binding groove which is critical to the interaction with RyR2 CaMBD2 [4,42]. In the absence of Ca^{2+}, the CaM C-domain binds part of RyR2 CaMBD2 around Phe-3603 (Figure 1E) via the C-domain's Met rich binding groove. In the presence of Ca^{2+}, the Ca^{2+}-bound CaM C-domain shifts to the C-terminal part of CaMBD2 (from Phe-3603 to Trp-3587), and the Ca^{2+}-bound CaM N-domain rotates approximately 180^{o} about the CaM linker that connects the N- and C-domain, and binds RyR2 CaMBD2 around Phe-3603 via its Met rich binding groove (Figure 1E-F) [17]. Here we mainly consider CaM's conformational changes, but noteworthy RyR2 also undergoes considerable conformational changes depending on the ligands present (Figure 1A-D).

The regions of RyR2 CaMBD2 that interact with CaM are fully resolved in the Ca^{2+}-saturated RyR2-CaM structure (Lys-3584 to Pro-3607, Figure 1F), but only the C-terminal part is resolved in the absence of Ca^{2+} (Ser-3592 to Pro-3607, Figure 1E). None of the three putative RyR2 CaMBDs are fully resolved in the current RyR2 structures, but their approximate locations can be inferred [17,22]. The 13 most N-terminal amino acids of RyR2 CaMBD1a are visible (Arg-1941 to Met-1953) and this region directly contacts the CaM C-domain, but not the CaM N-domain, in either RyR2-CaM conformation (Figure 1C-D). Approximately half of RyR2 CaMBD1b is resolved (Leu-2029 to Tyr-2038), and the location of CaMBD3 unfortunately remains obscure as it is within the Ser-4207 to Ile-4484 unresolved region. No direct contact between the CaM N-domain and CaMBD1a, -1b or -3 are observed. The cryo-EM structure is of the porcine RyR2, but the numbering used here refers to the corresponding human RyR2 amino acids as determined from the sequence alignments.

As a further evaluation of the RyR CaMBDs, we performed protein alignments of ryanodine receptor type 1-3, and also submitted the RyR2 protein sequence to the CaM-binding site search tool available from the CaM target database (CTD) [43]. Multiple protein sequence alignments showed that CaMBD1a and the canonical CaMBD2 are located within regions highly conserved between RyR1-3, whereas regions around CaMBD1b and especially CaMBD3 show significant differences between RyR isoforms (Figure 2). Moreover, RyR2 CaMBD3 is located within a region (Asp3790-Glu4562) previously designated as one of the three so-called divergent regions among RyR isoforms [5,44]. Analysing the RyR2 protein sequence for CaM-binding motifs using the CTD identified CaMBD2 and CaMBD3 as a 1-14-motif and a 1-5-10-motif, respectively [45]. In addition, a non-canonical CaM-binding site was identified within the CaMBD1b using a partial RyR2 sequence, Ala1240-Asn2700. Noteworthy, no CaM-binding site was predicted within RyR2 CaMBD1a.

The CaM-N54I mutation slightly decreases the binding of CaM to RyR2 CaMBD1a and -1b, but does not alter CaM binding to CaMBD2 and -3 peptides

To investigate whether CaM-N54I binding to RyR2 CaMBDs differs from that of the CaM-WT, we measured the affinity of CaM-WT and -N54I for binding to peptides representing each of the RyR2 CaMBDs (Table 2). Because these interactions are strongly dependent on the free Ca^{2+} concentration ($[Ca^{2+}]_{free}$), we measured CaM's affinity for binding to each peptide in a physiologically relevant $[Ca^{2+}]_{free}$ range (~0.05 – 400 μM) [46]. This was done by titrating fluorescently labelled peptides with CaM in $[Ca^{2+}]_{free}$-buffered solutions and monitoring the extent of CaM binding to the peptides using the change in peptide fluorescence anisotropy (FA). By fitting these FA titration curves to a stoichiometric binding model, we obtained the affinity of CaM for binding to each peptide expressed as that interaction's dissociation constant (K_D) at each $[Ca^{2+}]_{free}$ (Figure 3) [46]. A low K_D equates to extensive protein-peptide complex formation and thus a high-affinity interaction (see 'Materials and methods').

CaM-WT bound to the CaMBD2 peptide with a high affinity (K_D 1.2 nM – 1 μM) and the binding was strongly Ca^{2+}-dependent from 2 nM to 4 μM $[Ca^{2+}]_{free}$. The K_D for the interaction between CaM-WT and the CaMBD2 peptide decreased more than 330-fold from 0.05 to 4 μM $[Ca^{2+}]_{free}$ and no further decrease in K_D was observed above 4 μM $[Ca^{2+}]_{free}$. Similarly, CaM-WT also bound to the CaMBD3 peptide in a highly Ca^{2+}-dependent manner and with more than 1 μM $[Ca^{2+}]_{free}$, Ca-WT's affinity for binding the CaMBD3 peptide (K_D < 1 nM) was even higher than that of the CaM-WT-CaMBD2 interaction. The binding of CaM-N54I to the CaMBD2 peptide was not significantly different from that observed for CaM-WT at any $[Ca^{2+}]_{free}$, and this was also the case for the CaMBD3 peptide. Binding of CaM-WT to the RyR2 CaMBD1a and -1b peptides was also strongly Ca^{2+}-dependent, although binding was only detectable (K_D < 2 μM) from 0.4 μM and 2 μM $[Ca^{2+}]_{free}$, respectively (Figure 3). The K_D for CaM-WT binding to the RyR2 CaMBD1a peptide decreased 15-fold in the $[Ca^{2+}]_{free}$ range from 2 to 400 μM, and similarly the K_D for CaM-WT binding to the RyR2 CaMBD1b peptide decreased 10-fold in the range 0.4 to 400 μM $[Ca^{2+}]_{free}$. Binding of CaM-N54I to the RyR2 CaMBD1a and CaMBD1b peptides showed the same Ca^{2+}-dependency as the CaM-WT interaction. However, CaM-N54I had a significantly lower affinity for binding either of these RyR2 CaMBD peptides, compared to the CaM-WT (Table 3). Beginning at 2 μM $[Ca^{2+}]_{free}$ the K_D for CaM-N54I binding to the RyR2 CaMBD1a peptide was on average 1.4-fold higher than that for the CaM-WT (Figure 3 and Table 3). Similarly, beginning at 2 μM $[Ca^{2+}]_{free}$ the K_D for CaM-N54I binding to the RyR2 CaMBD1b peptide was on average 1.8-fold higher than the K_D for CaM-WT binding.

Taken together the results from titrations of RyR2 CaMBD peptides with either CaM-WT or -N54I showed that the N-domain N54I mutation slightly decreased CaM's affinity for binding to RyR2 CaMBD1a and -1b, albeit the mutation did not affect binding to RyR2 CaMBD2 or CaMBD3.

CaM-WT, but not CaM-N54I, decreases [^{3}H]ryanodine binding to RyR2 despite deletion of CaMBD1a, -1b or -3

A hall-mark of RyR2 channels is their binding to the agonist ryanodine [5,47]. Ryanodine binds with high affinity to RyR2 channels in their open conformation, and the RyR2-ryanodine association is therefore an indirect estimate of RyR2 open propensity [47,48]. To investigate the effect of CaM on this open propensity we measured the time-dependent binding of tritium ([^{3}H]) labelled ryanodine to lysates of RyR2-expressing HEK293 cells, without or with addition of CaM. Also, to investigate the significance of RyR2 CaMBDs for the effect of CaM on RyR2 ryanodine binding, we used the five different HEK293 cell lines expressing RyR2 variants with each CaMBD deleted (Table 1 and Figure 4). Binding experiments were done at 1 μM $[Ca^{2+}]_{free}$, and with either no added CaM (Ctrl) or addition of either CaM-WT or CaM-N54I (Figure 4A). Binding of [^{3}H]ryanodine to RyR2 variants was measured for different time points, and the resulting binding curves were fitted to a one-phase association model for determining the ryanodine association rate (K) and the total ryanodine binding at near equilibrium (B_{eq}).

Lysates from cells expressing RyR2-WT, -ΔCaMBD2 or -ΔCaMBD3 showed similar equilibrium ryanodine binding (average B_{eq} 119 ±12 counts·L·h^{-1}·g^{-1}), comparing reactions without additional CaM (Figure 4B). On the other hand, the binding curves for lysates with RyR2-ΔCaMBD1a or -ΔCaMBD1b showed an approximately 2-fold lower equilibrium ryanodine binding (B_{eq} 32±3 and 53±4 counts·L·h^{-1}·g^{-1}), compared to former three RyR2 variants. This difference in the fitted [^{3}H]ryanodine binding at equilibrium indicated that RyR2-ΔCaMBD1b and -ΔCaMBD1a bound ryanodine to a lesser extent than the other RyR2 variants at 1 μM $[Ca^{2+}]_{free}$. Nevertheless, the effect of CaM on [^{3}H]ryanodine binding could be investigated for all RyR2 variants by monitoring changes to the [^{3}H]ryanodine association rate in the absence or presence of CaM.

Addition of CaM-WT to the binding reactions with lysate containing RyR2-WT significantly decreased the [^{3}H]ryanodine association rate from 0.9 to 0.6 h^{-1} while addition of CaM-N54I did not affect the rate of binding (K 1.0 h^{-1}), compared to reactions without CaM added (Figure 4C). A tendency towards a slightly slower [^{3}H]ryanodine association rate was observed with the addition of CaM-N54I, compared to the Ctrl condition, but it was not statistically significant. Results similar to those for RyR2-WT were observed for cell lysates containing RyR2-ΔCaMBD1b or -ΔCaMBD3 i.e. addition of CaM-WT markedly decreased the [^{3}H]ryanodine association rate while addition of CaM-N54I only tended to decrease the association rate slightly

and not significantly. CaM-WT appeared to decrease the [^{3}H]ryanodine association rate more so when added to lysates with RyR2-ΔCaMBD3 than when added to RyR2-WT lysates, however this difference in magnitude of effect was not statistically significant. For lysates containing RyR2-ΔCaMBD1a, the same tendency for CaM-WT to decrease the [^{3}H]ryanodine association rate was observed, although the effect was not statistically significant. This lack of statistical significance was ascribed to the over-all [^{3}H]ryanodine binding to lysates with RyR2-ΔCaMBD1a being too low to adequately resolve potential differences in the binding curves. Addition of CaM-WT or -N54I to lysates containing RyR2-ΔCaMBD2 did not significantly affect the [^{3}H]ryanodine association rate, compared the reaction with no CaM added. Moreover, no significant differences were observed when comparing the [^{3}H]ryanodine association rates between the five different RyR2-variants without CaM addition i.e. the CaMBD deletions appeared not to significantly affect the rate of [^{3}H]ryanodine at 1 μM $[Ca^{2+}]_{free}$, compared to that for RyR2-WT.

Taken together, these results indicate that CaM-WT decreased [^{3}H]ryanodine binding to RyR2-WT, -ΔCaMBD1b and -ΔCaMBD3 whereas CaM-N54I did not, or only did so to a much lesser extent. The same tendency was observed for RyR2-ΔCaMBD1a, although definitive conclusions could not be made with this data set. Neither CaM-WT nor –N54I significantly affected [^{3}H]ryanodine binding to RyR2-ΔCaMBD2.

CaM-N54I diminishes CaM-dependent inhibition of RyR2-mediated store-overload induced Ca^{2+} release in HEK293 cells despite deletion of CaMBD1a, -1b or -3

For a more detailed investigation of the functional effects of the N54I mutation on the CaM-dependent inhibition of RyR2 Ca^{2+} release, with respect to the four CaMBDs, we measured the effect of CaM on store-overload induced Ca^{2+} release (SOICR) in HEK293 expressing each of the RyR2 variants (Table 1). To this end, we co-transfected RyR2-expressing HEK293 cells with the D1ER Ca^{2+} probe and either CaM-WT or CaM–N54I [7,8,39]. Extracellular perfusion of cells with 2 mM Ca^{2+} increased the endoplasmic reticulum (ER) free Ca^{2+} concentration (ER Ca^{2+} load) and caused SOICR such that the ER Ca^{2+} load oscillated with the concerted opening and closing of RyR2 channels (Figure 5). The activation threshold (ER Ca^{2+} load at SOICR initiation) and the termination threshold (the ER Ca^{2+} load at which Ca^{2+} release ceases) were determined from the oscillations in the D1ER probe's fluorescence resonance energy transfer (FRET) signal, and the difference (activation threshold – termination threshold) was the fractional ER Ca^{2+} release (Figure 5A) [7,41] – please see [39] for a graphical overview of the process. An increase in the activation threshold indicates that RyR2 channels are less sensitive to stimulation by ER luminal Ca^{2+}, and similarly an increase in the termination threshold indicates that channels are more susceptible to inactivation when open. Thus, increases in the RyR2

activation and/or termination thresholds indicate inhibition of RyR2 Ca^{2+} release, and accordingly so does a decrease in the fractional ER Ca^{2+} release.

The SOICR experiments were carried out with three different CaM conditions: control (i.e. only endogenous CaM), CaM-WT or CaM–N54I plasmid-mediated expression in each of the five different cell lines expressing either RyR2-WT, -ΔCaMBD1a, -ΔCaMBD1b, -ΔCaMBD2 or -ΔCaMBD3 (Figure 5 and Table 1). HEK293 cells endogenously express CaM, but transfecting HEK293 cells with a CaM expression plasmid increases the CaM protein level and thereby affects the CaM-dependent inhibition of RyR2 during SOICR (see Figure 10 in 'Materials and methods'). Transfection with a CaM-WT plasmid increases the observed RyR2 termination threshold whereas transfection with a CaM-N54I plasmid decreases both the activation and termination threshold, thereby markedly reducing CaM's inhibition of RyR2. Noteworthy, RyR2-ΔCaMBD2 is insensitive to the CaM expression conditions, which is consistent with the ablation of CaM-dependent RyR2 inhibition [7,8,16,39].

In this study, exogenous CaM-WT expression facilitated the inhibition of RyR2-WT by increasing the termination threshold 4 % (from 58 to 62 %), compared to the control, and thereby reduced the fractional ER Ca^{2+} release from 31 to 29 % (Figure 6B-C, Table 4). Conversely, CaM-N54I expression diminished RyR2-WT inhibition and increased fractional ER Ca^{2+} release (from 29 to 36 %) by lowering both the activation (from 90 to 85 %) and termination threshold (from 62 to 49 %), compared to CaM-WT expression (Figure 6A-C, Table 4). Although subtle, the inhibitory effect of CaM-WT expression on RyR2 Ca^{2+} release is consistently observed during SOICR in RyR2-expressing HEK293 cells [7,8,16,39]. The small but significant changes by exogenously expressed CaM-WT most likely reflect a greater saturation of RyR2 with CaM, thereby increasing the inhibition of RyR2 already exerted by endogenous CaM. In the same way, the expressed CaM-N54I can bind to unoccupied RyR2 CaMBD sites, and likely also to some extent replaces endogenous CaM-WT due to mutant protein abundance [7,8,16,39]. Plasmid expression of CaM-WT or CaM-N54I increased total CaM protein levels 2-fold in HEK293 cells, compared to endogenous CaM expression (see 'Materials and methods').

Compared to RyR2-WT, RyR2-ΔCaMBD1a showed a markedly increased activation threshold and this was true for all CaM expression conditions (Figure 6A, Table 4). Moreover, with only endogenous CaM (Ctrl) the termination threshold for RyR2-ΔCaMBD1a was clearly decreased compared to RyR2-WT (36 vs 58 %, Figure 6B). Because RyR2-ΔCaMBD1a had both an increased activation and a decreased termination threshold, the resulting fractional ER Ca^{2+} release increased 2-fold from 31 to 61 %, comparing the controls for RyR2-WT and RyR2-ΔCaMBD1a (Figure 6C). Remarkably, CaM-WT expression nearly rescued this excessive RyR2-ΔCaMBD1a Ca^{2+} release by prominently increasing the RyR2-ΔCaMBD1a termination

threshold from 36 to 57 %, compared to the control (Figure 6B-C). Compared to the effect of CaM-WT, CaM-N54I expression markedly decreased the termination threshold (from 57 to 42 %) and therefore increased the fractional ER Ca^{2+} release from 44 to 55 % (Figure 6A-C).

Unlike the observations made with RyR2-ΔCaMBD1a, the effects of deleting CaMBD1b were subtle although RyR2-ΔCaMBD1b showed a decreased activation threshold, compared to RyR2-WT, both with and without CaM expression (~ 84 vs. 90 %, Figure 6A). Compared to the control condition, CaM-WT expression increased the RyR2-ΔCaMBD1b termination threshold (63 vs. 58 %), and thereby minutely lowered the fractional ER Ca^{2+} release (22 vs 25 %). These effects of CaM-WT expression where highly similar to the effects of CaM-WT expression on RyR2-WT (Figure 6B-C), and similarly CaM-N54I expression also decreased the RyR2-ΔCaMBD1b termination threshold from 63 to 53 %, compared to CaM-WT expression. On the other hand, CaM-N54I expression did not significantly lower the RyR2-ΔCaMBD1b activation threshold as it did for RyR2-WT.

Interestingly, the inherent effects on the RyR2 activation threshold stemming from deleting either CaMBD1a (marked activation increase) or CaMBD1b (subtle activation decrease) appeared to occlude any further effects of CaM-N54I expression on the activation thresholds of either RyR2-ΔCaMBD1a or -ΔCaMBD1b. However, a tendency towards a slightly lowered activation threshold from CaM-N54I expression was observed for RyR2-ΔCaMBD1a and -ΔCaMBD1b, compared to CaM-WT expression.

RyR2-ΔCaMBD3 did not show any significant differences in the RyR2 Ca^{2+} release properties during SOICR, compared to RyR2-WT. Moreover, CaM-WT and CaM-N54I expression affected RyR2-ΔCaMBD3 the same as RyR2-WT (Figure 6A-C, Table 4). Collectively, the deletion of either CaMBD1a, -1b or -3 did not diminish the effect of either CaM-WT or CaM-N54I expression on RyR2 regulation during SOICR oscillations: CaM-WT expression increased CaM-dependent inhibition of RyR2 Ca^{2+} release, whereas CaM-N54I diminished RyR2 inhibition.

CaM-N54I diminishes CaM-dependent inhibition of RyR2-mediated Ca^{2+} release in permeabilized HEK293 cells with elevated cytosolic Ca^{2+}, despite deletion of CaMBD1a, -1b or -3

Ca^{2+} binding to CaM increases its inhibitory effect on RyR2, and most likely more than 1 μM $[Ca^{2+}]_{cyt}$ is required to fully saturate CaM with Ca^{2+} during its interaction with RyR2 [8,16]. During SOICR in HEK293 cells, $[Ca^{2+}]_{cyt}$ oscillates between approximately 0.05 – 2 μM i.e. only briefly reaches 1 μM [49,50] (time trace nadirs, Figure 5). To better investigate CaM-dependent RyR2 inhibition under elevated $[Ca^{2+}]_{cyt,}$ conditions, we used permeabilized HEK293 cells and a Ca^{2+}-buffered perfusion medium with a constant 1 μM $[Ca^{2+}]_{free}$.

Cytosolic 1 μM $[Ca^{2+}]_{free}$ strongly activates RyR2 and consequently reduces the ER Ca^{2+} load required for triggering SOICR, i.e. lowers the activation threshold. Under such conditions, RyR2 Ca^{2+} release does not cause oscillations in ER Ca^{2+} concentrations, but instead the ER Ca^{2+} load reaches a steady-state that likely reflects the opposing fluxes of RyR2 Ca^{2+} release and the SR/ER Ca^{2+} ATPase 2 (SERCA2b) Ca^{2+} uptake [51] – please see [39] for a graphical overview of the process. The D1ER Ca^{2+} probe FRET signal can then be used for measuring this steady-state ER Ca^{2+} load at a given perfusion condition (Figure 7) [39,52].

To measure the effect of CaM on RyR2 Ca^{2+} release, the steady-state ER Ca^{2+} load in permeabilized HEK293 cells expressing each of the RyR2 variants was measured first without CaM (endogenous CaM washed out) and then after the addition of either CaM-WT or -N54I (Figure 7, Figure 8 and Table 5). The removal of endogenous CaM during permeabilization was evident from the steady-state ER Ca^{2+} load for RyR2-WT and RyR2-ΔCaMBD2 (that abolishes CaM-dependent inhibition) being the same before the addition of CaM-WT (Figure 8 and Table 5), and also from the marked response of RyR2-WT to exogenous CaM addition.

Addition of exogenous CaM-WT to permeabilized cells expressing RyR2-WT increased the steady-state ER Ca^{2+} load 1.3-fold from 32 to 41 %, i.e. reduced ER Ca^{2+} release by inhibiting RyR2. Conversely, addition of CaM-N54I decreased the steady-state ER Ca^{2+} load 0.9-fold from 32 to 27 % and thus had the opposite effect compared to the addition of CaM-WT. In other words, CaM-N54I not only failed to inhibit but also facilitated RyR2-mediated Ca^{2+} release as evident from the steady-state ER Ca^{2+} with CaM-N54I being significantly below that observed without any CaM present. The observed facilitation of RyR2 Ca^{2+} release by CaM-N54I was similar to previous observations made for arrhythmogenic CaM C-domain mutations, although considerably smaller in magnitude [39,52]. In contrast to RyR2-WT, no significant effect on steady-state ER Ca^{2+} load was observed when adding CaM-WT to RyR2-ΔCaMBD2, and RyR2-ΔCaMBD2 has also previously been shown to be insensitive to regulation by CaM-N54I as well as other CaM mutants [7,8,39]. This result strongly supported that the effects of adding CaM-WT or -N54I to RyR2-WT were due to CaM regulating RyR2, and not secondary effects due to CaM affecting other protein targets.

The effect on steady-state ER Ca^{2+} load from adding CaM-WT to RyR2-ΔCaMBD1b or -ΔCaMBD3 expressing cells were not significantly different from the effect of adding CaM-WT to cells expressing RyR2-WT (group b, Figure 8A-B). Moreover, adding CaM-N54I to cells expressing RyR2-ΔCaMBD1b or -ΔCaMBD3 caused decreases in the steady-state ER Ca^{2+} load which were indistinguishable from the effects of adding CaM-N54I to RyR2-WT expressing cells (group c, Figure 8A-B). Hence, deleting RyR2 CaMBD1b or CaMBD3 did not significantly affect the native CaM-dependent inhibition of RyR2-mediated Ca^{2+} release at 1 μM cytosolic Ca^{2+}, nor did these deletions impede CaM-N54I in promoting RyR2 Ca^{2+} release.

The effects of adding CaM-WT or -N54I to cells expressing RyR2-ΔCaMBD1a were more complex (group d and *, Figure 8A-B). Addition of CaM-WT increased the steady-state ER Ca^{2+} load 1.7-fold from 31 to 54 %, and this was significantly greater than the 1.3-fold increase observed when adding CaM-WT to RyR-WT. In fact, the quantified increase caused by CaM-WT on the steady-state ER Ca^{2+} load in cells expressing RyR2-ΔCaMBD1a (21 %) was approximately double that observed with RyR2-WT (9.1 %). Interestingly, addition of CaM-N54I to RyR2-ΔCaMBD1a expressing cells did not decrease the steady-state ER Ca^{2+} load as observed for cells expressing RyR2-WT, -ΔCaMBD 1b and -ΔCaMBD3. Instead, CaM-N54I addition increased the steady-state ER Ca^{2+} load in cells expressing RyR2-ΔCaMBD1a 1.3-fold from 31 to 41 %, noteworthy this was a significantly smaller increase than conferred by the CaM-WT acting on RyR2-ΔCaMBD1a. At the same time this effect of CaM-N54I on the steady-state ER Ca^{2+} load was distinct from its effect on all other RyR2 expressing cells. However, given the inherent effect of CaMBD1a deletion on RyR2 activity (Figure 4B) and that RyR2-CaMBD1a appeared more susceptible for regulation by CaM (Figure 6), the main observation was that CaM-N54I still caused less inhibition of RyR2 than CaM-WT.

Taken together these results showed that CaM-WT strongly inhibited ER Ca^{2+} release in permeabilized cells expressing RyR2-WT, whereas CaM-N54I promoted ER Ca^{2+} release. Noteworthy, removing RyR2 CaMBD1b or CaMBD3 did not significantly change the effects on RyR2-mediated ER Ca^{2+} release conferred by CaM-WT or CaM-N54I. Deleting RyR2 CaMBD1a, however, increased the magnitude of the RyR2 inhibition conferred by CaM-WT two folds and caused CaM-N54I to exert a net inhibitory effect, although still less than the CaM-WT effect.

Deletion of CaMBD1a, CaMBD1b or CaMBD2 affects the response of RyR2 to caffeine activation

Results so far indicated that the deletions of CaMBD1a and to a lesser extent CaMBD1b inherently affected RyR2 ryanodine binding and Ca^{2+} release in our experiments. To further investigate the impact of RyR2 CaMBD deletions on channel function, we measured the response of each RyR2 variant to activation by caffeine through monitoring the bulk, cytosolic Ca^{2+} transients in HEK293 cells resulting from successive addition of caffeine. RyR2-mediated ER Ca^{2+} release strongly depends on the concentrations of ER luminal Ca^{2+}, and caffeine increases RyR2 propensity for activation by ER luminal Ca^{2+}. Thus, for each increase in caffeine concentration, the threshold for RyR2 activation by ER Ca^{2+} is lowered and Ca^{2+} is released into the cytosol until ER luminal Ca^{2+} again becomes lower than that needed for opening RyR2. Also, HEK293 cells maintain cytosolic Ca^{2+} homeostasis such that ER Ca^{2+} released is eventually cleared, and altogether this process results in a transient, cytosolic Ca^{2+} increase (peak) for each caffeine addition (Figure 9A). These peaks

were monitored using a cytoplasmic, fluorescent Ca^{2+} probe (Fluo-3), and peak the height as a function of cumulative caffeine concentration gave a caffeine response profile for each RyR2 variant (Figure 9B).

The caffeine response profiles showed that all RyR2 variants were sensitive to caffeine stimulation, and that the deletion of either CaMBD1a, CaMBD1b or CaMBD2 did affect RyR2's response to caffeine (Figure 9B). A leftward-shift in the profile of the caffeine-induced Ca^{2+} release for RyR2-ΔCaMBD1b, i.e. more of the ER-stored Ca^{2+} released at lower cumulative caffeine concentration, indicated an increased caffeine response compared to RyR2-WT. Conversely, a rightward-shift in the profile for RyR2-ΔCaMBD1a showed that this deletion mutant was less responsive to caffeine stimulation than RyR2-WT. Similarly, the RyR2-ΔCaMBD2 showed to have a slightly reduced sensitivity to caffeine specifically at high cumulative concentrations (> 1 mM). Finally, RyR2-ΔCaMBD3 channels displayed a response to caffeine indistinguishable from that of the RyR2-WT channels.

DISCUSSION

CaM is a central regulator of intracellular Ca^{2+} release and excitation-contraction coupling in cardiac cells, and mutations in CaM cause severe arrhythmias [4,20,53]. One erroneous regulation caused by the CaM mutations is a diminished CaM-dependent inhibition of RyR2-mediated Ca^{2+} release from the ER/SR Ca^{2+} store [4,8,16,20,27,31,39,40,53,54]. Our current model for the CaM-RyR2 interaction is that under cardiomyocyte resting conditions (~100 nM $[Ca^{2+}]_{cyt}$), the CaM C-domain is nearly saturated with Ca^{2+} and constitutively anchored to CaMBD2 around Trp-3587 whereas the CaM N-domain is not bound to Ca^{2+} or CaMBD2 and may interact with other RyR2 CaMBDs. Upon cardiomyocyte excitation the CaM N-domain binds Ca^{2+} as $[Ca^{2+}]_{cyt}$ increases and this changes its interaction with RyR2 CaMBDs, and with one possibility being that the Ca^{2+}-saturated CaM N-domain binds to RyR2 CaMBD2 around Phe-3603, as observed in cryo-EM structures with Ca^{2+} present [7,8,16-19,39,46]. Structures in the physiological resting state (closed RyR2 and only the CaM C-domain Ca^{2+}-loaded) are not available, and the effect of the CaM C-domain's shift from Phe-3607 to Trp-3587 on the Ca^{2+}-free CaM N-domain remains unknown. Moreover, none of the three putative RyR2 CaMBDs are fully resolved in the current structures. Noteworthy, cryo-EM studies represent a subset of possible RyR2 macro complex conformations, and also clearly demonstrate that these conformations shift considerably depending on the ligands present [5,17,22-24]. Thus, interactions between CaM and CaMBD1a, -1b or even -3 cannot be completely ruled out.

Disruption of the tripartite interaction between Ca^{2+}, the CaM C-domain and RyR2 CaMBD2 leads to excessive Ca^{2+} release which can cause arrhythmia or cardiomyopathy, and this likely explains the diminished RyR2 inhibition conferred by CaM C-domain mutations [7-9,11-13,16,39,53,55,56]. However, the CaM-N54I mutation is the only N-domain mutation of the fifteen known CaM mutations and seemingly has little or no effect on CaM interaction with CaMBD2 or CaM binding to Ca^{2+} [8,16,25,38-40,54], yet it markedly impairs CaM-dependent inhibition of RyR2 [8,16,25,27,34,38,40,57].

In this study we investigated whether an interaction between the CaM N-domain and RyR2 CaMBD1a, CaMBD1b or CaMBD3 may explain the diminished CaM-dependent RyR2 inhibition conferred by CaM-N54I. Simultaneously, this study also assessed the functional significance of the RyR2 CaMBDs in the regulation of RyR2 by CaM-WT [7,8,16,41]. To this end we expressed RyR2-WT and four deletion mutants with the RyR2 CaMBD1a, CaMBD1b, CaMBD2 or CaMBD3 removed (Table 1) and investigated the effect of both CaM-WT and CaM-N54I on the CaM-dependent inhibition of RyR2. In the protein-peptide binding assay, CaM-N54I had a significantly lower Ca^{2+}-dependent affinity for binding to the CaMBD1a and CaMBD1b peptides, but the same affinity for binding to the CaMBD2 or CaMBD3 peptides, compared to the CaM-WT. This indicated that the N54I mutation may affect the interaction between RyR2 CaMBD1a and CaMBD1b and the CaM N-domain

(Figure 3 and Table 3). Also, since both CaM-WT and CaM-N54I readily bound to RyR2 CaMBD1a, CaMBD1b and CaMBD3 peptides, these regions were expected to be relevant for CaM-dependent RyR2 regulation for both CaM variants. However, our experiments using SOICR in intact HEK293 cells showed that CaM-N54I conferred insufficient RyR2 inhibition during SOICR, compared to CaM-WT, despite deletions of either CaMBD1a, -1b or -3. Moreover, CaM-WT expression increased the inhibition of RyR2 Ca^{2+} release regardless of removing either CaMBD1a, -1b or -3 (Figure 6 and Table 4). Similarly, in experiments using permeabilized HEK293 cells with sustained 1 μM cytosolic side $[Ca^{2+}]_{free}$, addition of purified CaM-WT inhibited RyR2 Ca^{2+} release and CaM-N54I caused significantly less inhibition, despite deletion of either CaMBD1a, -1b or -3 (Figure 8 and Table 5). The apparent lack of effect of CaMBD deletions on CaM-dependent RyR2 inhibition was consistent with the lack of effect of CaMBD deletions on CaM-mediated decrease in [^{3}H]ryanodine binding to RyR2 (Figure 4).

Interestingly, CaM-N54I addition even promoted RyR2 Ca^{2+} release in permeabilised cells expressing RyR2-WT, -ΔCaMBD1b and -ΔCaMBD3, an effect previously observed for some CaM C-domain mutations [39]. The N54I mutation did not promote Ca^{2+} release in permeabilized cells expressing RyR2-ΔCaMBD1a but still decreased RyR2 inhibition, compared to CaM-WT. Therefore CaM-N54I appeared to diminish RyR2 inhibition less so in cells expressing RyR2-CaMBD1a, compared to RyR2-WT, -ΔCaMBD1b and -ΔCaMBD3. If removing CaMBD1a disrupted a RyR2-CaM N-domain interaction, CaM-WT and CaM-N54I should affect RyR2-ΔCaMBD1a similarly, but oppositely we found that the N54I mutation still diminished RyR2 inhibition, compared to CaM-WT. Thus, the difference in CaM-N54I's effect on RyR2-CaMBD1a, compared to RyR2-WT, -CaMBD1b and -CaMBD3, in permeabilised cells was instead considered a consequence of the CaMBD1a deletion itself (further details below).

Although CaMBD1a and CaMBD1b were not a requirement for CaM to inhibit RyR2, deleting either of these CaMBDs in itself altered RyR2 Ca^{2+} release. Removing CaMBD1a markedly reduced RyR2 activation by both SOICR and caffeine while simultaneously increasing ER Ca^{2+} release in intact cells by delaying channel closing, i.e. lowered the termination threshold (Figure 9B and Figure 6A-B). In other words, RyR2-ΔCaMBD1a appeared more resistant to activation than RyR2-WT, yet more prone to increased Ca^{2+} release once opened. This suggests that the region around RyR2 CaMBD1a, and by extension the CaM binding region around CaMBD2 (Figure 1), may play a role in RyR2 transitioning between open and closed conformations. This is further supported by studies comparing RyR cryo-EM structures, and that RyR2 CaMBD1a interacts directly with the CaMBD2-bound CaM C-domain in RyR2-CaM structures [5,17,23]. The inhibitory effect of CaM-WT or CaM-N54I on RyR2-ΔCaMBD1a (21 % and 15 %) appeared much greater than their effects on RyR2-WT (9.1 % and -3.7 %) in permeabilized cells with 1 μM cytosolic $[Ca^{2+}]_{free}$ (Figure 8B). The

explanation for this observation is unknown, but we speculate that the decreased sensitivity of RyR2-ΔCaMBD1a for activation possibly allows a stronger CaM-mediated inhibition due to less contending RyR2 Ca^{2+} stimulation. Removing CaMBD1b promoted RyR2 activation as seen from the decreased SOICR activation threshold and the increased sensitivity to caffeine (Figure 9B and Figure 6A-B). However, these effects were subtle compared to removing CaMBD1a, and there was no significant effect of removing CaMBD1b on steady-state ER Ca^{2+} load in permeabilized cells (Figure 8B).

In summary, we find that under our experimental conditions neither CaMBD1a, -1b nor -3 are strictly necessary for CaM-dependent RyR2 inhibition and comparing the effect of CaM-WT to that of CaM-N54I there are no significant indications that the CaM N-domain interacts with CaMBD1a, CaMBD1b or CaMBD3. I.e. a CaM N-domain interaction with either CaMBDa1, CaMBD1b or CaMBD3 is not the underlying mechanism for CaM-N54I's aberrant regulation of RyR2. Interestingly, our results indicate that CaM primarily regulates RyR2 via CaMBD2 or regions other than CaMBD1a, -1b and -3, but also support that CaMBD1a is integral to RyR2 regulation possibly through allosteric modulation of CaM binding. The results presented here and in previous studies show that RyR2 CaMBD2 is indeed required for CaM-N54I to interact with RyR2 via the CaM C-domain, but it is unlikely that the N-domain N54I mutation confers erroneous RyR2 regulation via CaMBD2 because the N54I mutation does not affect the CaM-RyR2 CaMBD2 interaction [8,16,25]. Thus, given that RyR2 CaMBD1a, -1b or -3 are not strictly required for CaM-dependent regulation of RyR2, and that CaM-N54I interacts with Ca^{2+} and RyR2-CaMBD2 indistinguishably from the CaM-WT, we propose that the N54I mutation impairs CaM-dependent RyR2 inhibition through an unknown CaMBD. CaM-N54I's diminished inhibition of RyR2 persisted even in the presence of Ca^{2+} (Figure 4 and Figure 8) [8,16,40,57], and therefore the newly identified region in the RyR2-CaM structure in the absence of Ca^{2+} that interacts with the CaM-N-domain was not considered a good candidate for this unknown CaMBD. Notable, the molecular details of how the N54I mutation diminishes CaM-dependent RyR2 inhibition still remain elusive, and therefore a so-far unobserved perturbation of the CaM-RyR2 CaMBD2 interaction cannot be entirely ruled out, even though the currently available data does not support this.

To our knowledge this study is the first to investigate the functional significance of RyR2 CaMBDs, other than CaMBD2, using intact RyR2 channels and *in vivo* ER Ca^{2+} release [5,15,46]. The RyR2-expressing HEK293 cells approximate diastole- and early systole-like Ca^{2+} conditions in cardiomyocytes, and has repeatedly proven a valid model for investigating perturbations of intracellular Ca^{2+} signalling [41,58-62]. Thus, this study supports that CaMBD1a, CaMBD1b and CaMBD3 are not required for CaM's inhibition of RyR2 Ca^{2+} release at low cytosolic Ca^{2+} levels. However, it is still possible that CaMBD1a, -1b and -3

contribute to CaM-dependent RyR2 regulation under certain conditions and $[Ca^{2+}]_{cyt}$ not obtainable in HEK293 cells, although this remains to be investigated.

MATERIALS AND METHODS

Ryanodine receptor protein sequence alignment

For protein sequence alignment, fifteen RyR sequences from human, mouse and rabbit RyR1-3, chicken RyR2-3, zebrafish RyR1b, *C. elegans* RyR, *D. melanogaster* RyR and *O. dioica* RyR were aligned using the ClustalW algorithm in CLC Main Workbench 6 (CLC Bio, version 6.9.1) [63]. UniprotKB file accession numbers: **P21817**, **Q92736**, **Q15413**, **E9PZQ0**, **E9Q401**, **A2AGL3**, **P11716**, **P30957**, **Q9TS33**, **F1NLZ9**, **Q90985**, **A6P4B8**, **P91905**, **Q24498**, **E4XPI8**. Delimitation of the protein regions corresponding to CaMBD1a, CaMBD1b, CaMBD2 and CaMBD3 were adopted from previous studies [9,15,46,64,65]. For further evaluation of the four CaMBDs, the human RyR2 protein sequence was submitted to binding site search tool which is part of the CaM Target Database [43]. Using this analysis tool, high scoring hits for CaM-binding motifs, like those in CaMBD2 and -3, may mask less prominent motifs. Therefore, a partial sequence of human RyR2 (Ala1240-Asn2700) was separately submitted to the analysis tool for the detailed analysis of CaMBD1a and -1b.

Plasmids and mutagenesis

The pcDNA3.1 (Thermo Fisher Scientific, Waltham, MA, USA) plasmids with CaM or CaM-N54I cDNA inserts for CaM expression in HEK293 cells [8], and the pcDNA3 (Thermo Fisher Scientific) plasmid encoding the D1ER Ca^{2+} probe have been described previously [7,41,66]. pMAL plasmids (New England Biolabs, Ipswich, MA, USA) used for expression of CaM variants in E. coli were described previously [25].

The construction of a pBluescript (Agilent, Santa Clara, California, USA) plasmid carrying mouse RyR2 cDNA has been described previously [67]. RyR2-WT and a variant with CaMBD2 deleted (RyR2-ΔCaMBD2) were available from previous studies [7,8], and for this study we made three novel RyR2 variants (RyR2-ΔCaMBD1a, -ΔCaMBD1b and -ΔCaMBD3). This was done using overlap-extension PCR to remove from the pcDNA3-RyR2 plasmid, the nucleotide sequences corresponding to the protein regions outlined in Table 1, as previously described [68,69]. Briefly, a NruI/EcoRV fragment containing ΔCaMBD1a or ΔCaMBD1b was generated by overlapping PCR. This fragment was then used to replace the corresponding WT fragment in the NheI/BsiwI fragment in pBluescript. The DNA fragment containing the deletion was then subcloned into the full-length mRyR2 in pcDNA5/FRT/TO (Thermo Fisher Scientific) using NheI and BsiWI. An MluI/Bsu36I fragment containing ΔCaMBD3 was also generated using the overlap PCR. These fragments were used to replace the corresponding WT fragment in the BsiwI/NotI fragment of RyR2 in pBluescript. The BsiwI/NotI fragment containing the CaMBD3 deletion was used to replace the corresponding WT fragment in the full-length mRyR2 in pcDNA5/FRT/TO. All deletions were confirmed by DNA sequencing.

Protein Expression and Purification

CaM-WT and -N54I were expressed from pMAL in E. coli Rosetta B cells (Merck, Darmstadt, Hesse, Germany) and purified as previously described [8,15,25]. The identity, purity, and integrity of each protein preparation were confirmed by SDS-PAGE and MALDI-TOF mass spectrometry of trypsin digested proteins. Protein concentrations were measured using absorption at 280 nm (extinction coefficient 2560 $cm^{-1}M^{-1}$).

Peptides corresponding to RyR2 CaMBDs

Peptides with an N-terminal 5-TAMRA (5-carboxytetramethylrhodamine) label and corresponding to RyR2 CaMBDs were from Proteogenix (Schiltigheim, France) at > 95 % purity (Table 2). Peptide concentrations were determined from the 5-TAMRA absorption at 556 nm (extinction coefficient 103.000 $cm^{-1}M^{-1}$). Stock solutions (~600 µM) were kept in 5 % acetonitrile and 0.1 % trifluoroacetic acid.

pH- and Ca^{2+}-buffered solutions

pH- and Ca^{2+}-buffered solutions (pCa-buffer) were prepared as previously described [39,70], and contained 50 mM HEPES, 100 mM KCl, 0.3 mM tris(2-carboxyethyl)phosphine, 0.5 mM ethylene glycol-bis(2-aminoethylether)-tetraacetic acid (EGTA), 1 mM free Mg^{2+} and 2 mM nitrilotriacetic acid (NTA) at pH 7.2 (25 °C) with variable concentrations of $CaCl_2$. Mixing various amounts of the pCa-buffers with and without 3 mM $CaCl_2$ to different $[Ca^{2+}]_{tot}$ established defined EGTA/NTA-buffered $[Ca^{2+}]_{free}$ [70]. The calculated buffer ionic strength was 156 mM, and the $[Ca^{2+}]_{free}$ was verified using the Ca^{2+} probe Fura-2 (Thermo Fisher Scientific) and binding of Ca^{2+} to free CaM [8,46,70].

Titrations of CaMBD peptides with CaM at discrete Ca^{2+} concentrations

A two-dimensional titration assay was used to determine the affinity of CaM for binding to the RyR2 CaMBD peptides at 16 discrete $[Ca^{2+}]_{free}$ as previously described [39,46]. Briefly; The binding of CaM to peptides was monitored as the change in the fluorescence anisotropy (FA) signal from the TAMRA-labelled peptides, and the titrations were done in 384-well microtiter plates (#3575, Corning, New York, NY, USA) with the peptide concentrations kept constant (~50 nM) and varying the CaM concentration. Using the pCa-buffers (see above) allowed for mixing high and low $[Ca^{2+}]_{tot}$ solutions to obtain specific $[Ca^{2+}]_{free}$ [70]. Each microtiter plate contained 24 titration points (CaM to peptide ratios) at each of the 16 different $[Ca^{2+}]_{free}$ (24 columns by 16 rows). CaM concentrations covered the range 0.2 nM – 18 µM, and $[Ca^{2+}]_{free}$ the range 0.3 nM – 400 µM.

Immediately after mixing, the FA signal was measured in a fluorescence plate reader (Infinite M1000, Tecan, Zurich, Switzerland). Mixings and FA measurements were done in triplicates at 25°C.

Titration curve analysis for determining the affinity of CaM for binding to CaMBD peptides

CaM binds RyR2 CaMBD peptides (P) stoichiometrically [15] with the binding affinity expressed as the apparent CaM/CaMBD complex (PCaM) dissociation constant (K_D) i.e.

$$PCaM \leftrightarrows P + CaM$$

$$K_D = \frac{[P] \cdot [CaM]}{[PCaM]}$$

where [P], [CaM] and [PCaM] are the concentrations of free CaMBD, free CaM, and CaM/CaMBD complex, respectively. This simple binding model assumes one type of CaM-CaMBD interaction i.e. characterized by one K_D, and the fractional saturation (Y) of CaMBD with CaM is then

$$Y = \frac{[PCaM]}{[P]_{tot}} = \frac{K_D + [P]_{tot} + [CaM]_{tot}}{2 \cdot [P]_{tot}} - \sqrt{\left(\frac{K_D + [P]_{tot} + [CaM]_{tot}}{2 \cdot [P]_{tot}}\right)^2 - \frac{[CaM]_{tot}}{[P]_{tot}}} \quad (1)$$

where $[P]_{tot}$ and $[CaM]_{tot}$ are the total concentrations of CaMBD peptide and CaM, respectively. For each plate row a titration curve of FA as a function of $[CaM]_{tot}$ was obtained. The measured FA signal consists of the FA signal from the free CaMBD peptide (FA_P) and the FA signal from the CaM/CaMBD complex (FA_{PCaM}), hence

$$FA = FA_P \cdot (1 - Y) + FA_{PCaM} \cdot Y \quad (2)$$

where FA_P and FA_{PCaM} represent the minimum (entirely free CaMBD peptide) and maximum (entirely bound CaMBD peptide) FA signal. Substituting the expression for Y in equation 1 for Y in equation 2 allowed for fitting the binding model to each titration curve and thus obtaining a K_D at that $[Ca^{2+}]_{free}$. The method allows reliable fitting of K_D values in the approximate range 1 nM – 2 μM [46].

CaM binding to RyR2 CaMBD1a does not fit the model in equation 1, but rather a stochiometric interaction with two different modes of CaM binding to CaMBD1a, a high affinity and a low affinity, each characterized by their own K_D (K_{DI} and K_{DII}) [46], and where Y is defined as

$$Y = \left(\frac{[CaM]}{K_{DI} + [CaM]} + \frac{[CaM]}{K_{DII} + [CaM]}\right) \quad (3)$$

For low affinity interactions $[CaM] \approx [CaM]_{tot}$ is a good approximation, and model fitting for CaMBD1a was done with this alternate expression for Y in equation 2. We considered only the first mode of CaM-CaMBD1a interaction with the highest affinity (i.e. K_{DI}). K_D (or K_{DI}) as a function of $[Ca^{2+}]_{free}$ was obtained by fitting each row-wise titration curve using non-linear regression in GraphPad Prism 6.07. Differences in the fitted K_D or KD_I values for CaM-WT compared to CaM-N54I were evaluated using multiple (one for each $[Ca^{2+}]_{free}$) unpaired t-tests with Holm-Sidak correction for multiple comparisons ($p < 0.05$ considered

significant). For statistically significant differences, the change in standard (1 M and 25 °C) Gibb's free energy of binding ($\Delta\Delta G^o$) was calculated as

$$\Delta\Delta G^o = -R \cdot T \cdot \ln\left(\frac{K_{D,\,CaM-WT}}{K_{D,\,CaM-N54I}}\right)$$

Generation of stable and inducible HEK293 cell lines

Genomic modified and inducible HEK293 cell lines for expressing mouse RyR2 and variants were generated using the Flp-In T-REx Core Kit (Thermo Fisher Scientific) as previously described [7]. This recombinase mediated approach integrates the RyR2 cDNA under control of a tetracycline inducible promoter into the flpase recognition target site in the HEK293 Flp-In cell line genome.

[^{3}H]ryanodine binding to RyR2 in HEK293 cell lysates

HEK293 cell lysates were prepared from cell lines induced to express the RyR2 variants as previously described [71], and total protein content estimated using the Protein Assay (BioRad, Hercules, California, USA). [^{3}H]ryanodine binding at 1 μM $[Ca^{2+}]_{free}$ was done using 0.5-0.8 g/L total protein from cell lysate in binding buffer (350 mM KCl, 25 mM Tris, 50 mM HEPES, 5 nM [^{3}H]ryanodine, 2.5 mM DTT, 0.5 mM EGTA, 0.47 mM $CaCl_2$ with protease inhibitors including 2.5 mM DTT, pH 7.4). The reaction time was varied by spacing additions of [^{3}H]ryanodine to otherwise pre-mixed samples. All reactions were then stopped together, and bound [^{3}H]ryanodine was quantified using liquid scintillation counting as previously described [71]. Background [^{3}H]ryanodine binding - corresponding to reaction time 0 h - was measured using the addition of 50 μM unlabelled ryanodine. Binding curves with four time points were done for each RyR2 variant, and both without and with the addition of either 7.5 μM purified CaM-WT or -N54I. The measured [^{3}H]-activity was normalized to the lysate total protein concentration, and four replicates for each combination of RyR2 and CaM conditions were done. The resulting binding curves were fitted to a one-phase association reaction (Figure 4A)

$$\mathrm{Y(t)} = \mathrm{Y(0)} + B_{\mathrm{eq}} \cdot \left(1 - \mathrm{e}^{-\mathrm{K}\cdot\mathrm{t}}\right)$$

, where Y is the measured [^{3}H]-activity, K is the association rate, and B_{eq} is the change in Y from Y(0) to saturation i.e. the [^{3}H]-activity when the reaction reaches equilibrium. For each RyR2 variant, the fitted values for K were compared using one-way ANOVA with Holm-Sidak's multiple comparisons correction, $p < 0.05$ considered significant. Using the same approach, the fitted values for the B_{eq} were compared between RyR2 variants for reactions without CaM added.

Endoplasmic reticulum luminal Ca^{2+} imaging of HEK293 cells expressing RyR2 during Store-Overload Induced Ca^{2+} Release (SOICR)

Single-cell endoplasmic reticulum (ER) luminal Ca^{2+} imaging of HEK293 cells expressing RyR2 variants was done as previously described [7]. Briefly, HEK293 cells stably expressing murine RyR2 variants were co-transfected with plasmids encoding CaM and the D1ER Ca^{2+} probe. The D1ER FRET signals, reflecting ER luminal free Ca^{2+} in individual cells, were monitored using an epi-fluorescent microscope during perfusion [7,62]. High extracellular Ca^{2+} concentration (2 mM) increased ER Ca^{2+} load, ultimately causing ER Ca^{2+} load oscillations due to RyR2 SOICR (Figure 5A and caption). The oscillating D1ER FRET signal time trace from each cell was used to measure the Ca^{2+} release properties of the RyR2 channels relative to the ER Ca^{2+} store capacity: the activation and termination thresholds, and with their difference taken as the fractional ER Ca^{2+} release (Figure 5A). The ER Ca^{2+} store capacities were calculated from the difference between FRET signal's maximum and minimum (F_{max} - F_{min}). Three different CaM expression conditions were used with each of the RyR2-ΔCaMBD variants (Table 1): endogenous CaM, and plasmid expression of either CaM or -N54I. An average measurement included imaging of 2-4 cover slips each yielding 5-20 single-cell FRET time traces, and 2-3 sets of measurements were done for each combination of RyR2 and CaM variants. The RyR2 Ca^{2+} release properties calculated for each of these time traces were aggregated to one data set (Table 4).

The measured RyR2 Ca^{2+} release properties passed a normality test (D'Agostino-Pearson) and were compared using two different one-way ANOVAs with Dunnett's correction for multiple comparisons, $p < 0.05$ considered significant. One test was done for the effect of each RyR2 mutation within each CaM-expression condition with values compared to those for RyR2-WT. And then a second test for the effect of each of the three CaM expression conditions within each RyR2 variant with values compared to those for **t**he condition with CaM plasmid expression. The purpose of the double analysis was to investigate both inherent effects of the RyR2 mutations and**,** separately**,** the effect of CaM-expression on each RyR2 variant. All the measured store capacities were evaluated using a one-way ANOVA with a Tukey's multiple comparisons correction for all possible combinations with no significant differences identified. All data points used for statistical analysis and figure plotting are available as supplemental data (Supplemental_data_table_1.csv).

HEK293 cells have an endogenous ER Ca^{2+} release mechanism mediated by the inositol triphosphate receptor. However, cells not modified for RyR2-expression do not show any changes in ER Ca^{2+} load under the conditions used to induce RyR2-mediated SOICR [7,41,50,66].

Estimation of CaM expression levels in HEK293 Cells

HEK293 cells expressing RyR2-WT were cultured as described above, and cell lysates prepared from the plasmid transfected cells were used for Western blotting for CaM as previously described (Figure 10) [16]. The primary antibodies Ab124742 (Abcam, Cambridge, UK) and A5316 (MilliporeSigma, Massachusetts, USA) were used for detecting CaM and actin. CaM and acting protein band intensities on the Western-blotted membranes were quantified using ImageJ, and the protein levels of total CaM in individual samples were normalized to that of β-actin [16,72]. Western blot analysis was done in triplicates, and expressions levels were compared for all possible combinations using one-way ANOVA with a Tukey multiple comparisons correction, $p < 0.05$ considered significant. Plasmid expression of either CaM-WT or CaM-N54I significantly increased total CaM protein 2-fold 1.8-fold (+/- 0.3) compared to endogenous CaM protein levels (Ctrl). No significant difference in the total CaM protein level was observed comparing plasmids expression of CaM-WT and CaM-N54I.

Endoplasmic reticulum luminal Ca^{2+} imaging of permeabilized HEK293 cells Expressing RyR2 with sustained 1 μM cytosolic Ca^{2+}

Measurements of permeabilized HEK293 single cell's steady-state ER Ca^{2+} load during perfusion with sustained 1 μM $[Ca^{2+}]_{free}$ was done as previously described with modifications [39,52]. Briefly, RyR2 expressing HEK293 cells were permeabilized by perfusion with 0.25 g/L saponin in Ca^{2+} free intracellular-like medium (ICM: 125 mM KCl, 19 mM NaCl, 10 mM HEPES, 2 mM ATP, 2 mM $MgCl_2$, and 50 μM EGTA at pH 7.4) for 1-2 min. The extent of permeabilization was continuously monitored and then halted by switching to ICM with 0.1 μM $[Ca^{2+}]_{free}$ for another 4 min. The D1ER FRET signal from single cells was then recorded during five different perfusion conditions (Figure 7): 0.1 μM $[Ca^{2+}]_{free}$, 1 μM $[Ca^{2+}]_{free}$, 1 μM $[Ca^{2+}]_{free}$ + 0.5 μM purified CaM, 0.1 μM $[Ca^{2+}]_{free}$ + 1 mM tetracaine and finally 0.1 μM $[Ca^{2+}]_{free}$ + 10 mM caffeine, all in ICM. All perfusions were done for 6 min, except for ICM with 0.1 μM $[Ca^{2+}]_{free}$ which was for 4 min. Perfusion rate was ~1.5 mL/min into an ~0.5 mL perfusion chamber. The first steps with permeabilization and perfusion without Ca^{2+} washed out endogenous CaM as evident from the stable steady-state ER Ca^{2+} load obtained at 1 μM $[Ca^{2+}]_{free}$ before the addition of CaM [39].

An average measurement included imaging of 1-2 cover slips each yielding 5-10 single-cell FRET time traces, and 2 sets of measurements were done for each combination of RyR2 and CaM variants (Table 5). The steady-state ER Ca^{2+} load was measured as the 1 min averaged FRET signal at the end of each perfusion step relative to the ER store capacity (Figure 7 and caption). All the measured steady-state ER Ca^{2+} loads were compared for all possible combinations using a Kruskal-Wallis test with a Dunn's multiple comparisons

correction, $p < 0.05$ considered significant. All data points used for statistical analysis and figure plotting are available as supplemental data (Supplemental_data_table_2.csv).

Caffeine induced Ca^{2+} release in HEK293 cells

Using the fluorescence Ca^{2+} indicator Fluo-3 AM (#F1221, Thermo Fischer Scientific), bulk cytosolic Ca^{2+} concentration was monitored in suspensions of RyR2-expressing HEK293 cells during caffeine additions, as previously described with minor modifications [52]. Briefly, HEK293 cell lines modified for expressing RyR2 variants were grown on 10 cm culture dishes (#83.3902, Sarstedt, Nümbrecht, North Rhine-Westphalia, Germany) until ~80 % confluence and the RyR2 expression induced by changing medium to one supplemented with 1 μg/mL tetracycline. After ~24 h of induced growth, cells were detached and loaded with Fluo-3 AM before wash with buffer. The Fluo-3 fluorescence was continuously measured in a spectrofluorometer (SLM-Aminco series 2) during repeated additions of caffeine. Caffeine addition elicited a RyR2-mediated Ca^{2+} release which transiently increased $[Ca^{2+}]_{cyt}$, i.e. a Fluo-3 fluorescence peak, and additions were spaced 90 s for $[Ca^{2+}]_{cyt}$ to return to basal levels before next addition (Figure 9A). Time traces of Fluo-3 fluorescence were normalized to the initial fluorescence intensity and a baseline correction done for each addition-segment to correct for cell suspension dilution ($\Delta F/F_0$) and caffeine fluorescence quenching. The caffeine response peak heights were measured for each addition, normalized to the maximum peak height in each trace, and plotted as normalized peak heights as a function of the cumulative caffeine concentration (Figure 9B). Significant differences in the caffeine responses between RyR2 and deletion variants were evaluated, at each cumulative caffeine concentration, using two-way ANOVA with a Dunnett's multiple comparisons correction, $p < 0.05$ considered significant. Using the integrated peak areas, instead of maximum heights, gave identical results (not shown). Measurements were done in at least triplicates.

REFERENCES

1 Fearnley CJ, Roderick HL & Bootman MD (2011) Calcium signaling in cardiac myocytes. *Cold Spring Harb Perspect Biol* **3**, a004242–a004242.

2 Bers DM (2008) Calcium cycling and signaling in cardiac myocytes. *Annu. Rev. Physiol.* **70**, 23–49.

3 Bers DM (2014) Cardiac sarcoplasmic reticulum calcium leak: basis and roles in cardiac dysfunction. *Annu. Rev. Physiol.* **76**, 107–127.

4 Sorensen AB, Søndergaard MT & Overgaard MT (2013) Calmodulin in a heartbeat. *FEBS J.* **280**, 5511–5532.

5 Yuchi Z & Van Petegem F (2016) Ryanodine receptors under the magnifying lens: Insights and limitations of cryo-electron microscopy and X-ray crystallography studies. **59**, 209–227.

6 Fruen BR, Black DJ, Bloomquist RA, Bardy JM, Johnson JD, Louis CF & Balog EM (2003) Regulation of the RYR1 and RYR2 Ca^{2+} release channel isoforms by Ca^{2+}-insensitive mutants of calmodulin. *Biochemistry* **42**, 2740–2747.

7 Tian X, Tang Y, Liu Y, Wang R & Chen SRW (2013) Calmodulin modulates the termination threshold for cardiac ryanodine receptor-mediated Ca^{2+} release. *Biochem. J.* **455**, 367–375.

8 Søndergaard MT, Tian X, Liu Y, Wang R, Chazin WJ, Chen SRW & Overgaard MT (2015) Arrhythmogenic Calmodulin Mutations Affect the Activation and Termination of Cardiac Ryanodine Receptor Mediated Ca^{2+} Release. *J Biol Chem*, jbc.M115.676627.

9 Yamaguchi N, Xu L, Pasek DA, Evans KE & Meissner G (2003) Molecular basis of calmodulin binding to cardiac muscle Ca^{2+} release channel (ryanodine receptor). *Journal of Biological Chemistry* **278**, 23480–23486.

10 Xu L & Meissner G (2004) Mechanism of calmodulin inhibition of cardiac sarcoplasmic reticulum Ca^{2+} release channel (ryanodine receptor). *Biophys J* **86**, 797–804.

11 Yamaguchi N, Takahashi N, Xu L, Smithies O & Meissner G (2007) Early cardiac hypertrophy in mice with impaired calmodulin regulation of cardiac muscle Ca release channel. *J Clin Invest* **117**, 1344–1353.

12 Arnáiz-Cot JJ, Damon BJ, Zhang X-H, Cleemann L, Yamaguchi N, Meissner G & Morad M (2013) Cardiac calcium signalling pathologies associated with defective calmodulin regulation of type 2 ryanodine receptor. *J. Physiol. (Lond.)* **591**, 4287–4299.

13 Yang Y, Guo T, Oda T, Chakraborty A, Chen L, Uchinoumi H, Knowlton AA, Fruen BR, Cornea RL, Meissner G & Bers DM (2014) Cardiac myocyte Z-line calmodulin is mainly RyR2-bound, and reduction is arrhythmogenic and occurs in heart failure. *Circ Res* **114**, 295–306.

14 Yamaguchi N, Chakraborty A, Huang T-Q, Xu L, Gomez AC, Pasek DA & Meissner G (2013) Cardiac hypertrophy associated with impaired regulation of cardiac ryanodine receptor by calmodulin and S100A1. *Am. J. Physiol. Heart Circ. Physiol.* **305**, H86–94.

15 Lau K, Chan MMY & Van Petegem F (2014) Lobe-specific calmodulin binding to different ryanodine receptor isoforms. *Biochemistry* **53**, 932–946.

16 Søndergaard MT, Liu Y, Larsen KT, Nani A, Tian X, Holt C, Wang R, Wimmer R, Van Petegem F, Fill M, Chen SRW & Overgaard MT (2016) The Arrhythmogenic Calmodulin p.Phe142Leu Mutation Impairs C-domain Ca^{2+}-binding but not Calmodulin-dependent Inhibition of the Cardiac Ryanodine Receptor. *J Biol Chem*, jbc.M116.766253.

17 Gong D, Chi X, Wei J, Zhou G, Huang G, Zhang L, Wang R, Lei J, Chen SRW & Yan N (2019) Modulation of cardiac ryanodine receptor 2 by calmodulin. *Nature* **245**, C1.

18 Maximciuc AA, Putkey JA, Shamoo Y & Mackenzie KR (2006) Complex of calmodulin with a ryanodine receptor target reveals a novel, flexible binding mode. **14**, 1547–1556.

19 Rodney GG, Moore CP, Williams BY, Zhang JZ, Krol J, Pedersen SE & Hamilton SL (2001) Calcium binding to calmodulin leads to an N-terminal shift in its binding site on the ryanodine Receptor. *Journal of Biological Chemistry* **276**, 2069–2074.

20 Walweel K, Oo YW & Laver DR (2017) The emerging role of calmodulin regulation of RyR2 in controlling heart rhythm, the progression of heart failure and the antiarrhythmic action of dantrolene. *Clin. Exp. Pharmacol. Physiol.* **44**, 135–142.

21 Chin D & Means AR (2000) Calmodulin: a prototypical calcium sensor. *Trends Cell Biol.* **10**, 322–328.

22 Peng W, Shen H, Wu J, Guo W, Pan X, Wang R, Chen SRW & Yan N (2016) Structural basis for the gating mechanism of the type 2 ryanodine receptor RyR2. *Science* **354**, aah5324–aah5324.

23 Bai X-C, Yan Z, Wu J, Li Z & Yan N (2016) The Central domain of RyR1 is the transducer for long-range allosteric gating of channel opening. *Cell Res.* **26**, 995–1006.

24 Yan Z, Bai X-C, Yan C, Wu J, Li Z, Xie T, Peng W, Yin C-C, Li X, Scheres SHW, Shi Y & Yan N (2015) Structure of the rabbit ryanodine receptor RyR1 at near-atomic resolution. **517**, 50–55.

25 Nyegaard M, Overgaard MT, Søndergaard MT, Vranas M, Behr ER, Hildebrandt LL, Lund J, Hedley PL, Camm AJ, Wettrell G, Fosdal I, Christiansen M & Børglum AD (2012) Mutations in calmodulin cause ventricular tachycardia and sudden cardiac death. *Am. J. Hum. Genet.* **91**, 703–712.

26 Limpitikul WB, Dick IE, Joshi-Mukherjee R, Overgaard MT, George AL & Yue DT (2014) Calmodulin mutations associated with long QT syndrome prevent inactivation of cardiac L-type Ca(2+) currents and

promote proarrhythmic behavior in ventricular myocytes. *Journal of Molecular and cellular cardiology* **74**, 115–124.

27 Hwang H-S, Nitu FR, Yang Y, Walweel K, Pereira L, Johnson CN, Faggioni M, Chazin WJ, Laver D, George AL, Cornea RL, Bers DM & Knollmann BC (2014) Divergent regulation of ryanodine receptor 2 calcium release channels by arrhythmogenic human calmodulin missense mutants. *Circ Res* **114**, 1114–1124.

28 Marsman RF, Barc J, Beekman L, Alders M, Dooijes D, van den Wijngaard A, Ratbi I, Sefiani A, Bhuiyan ZA, Wilde AAM & Bezzina CR (2014) A mutation in CALM1 encoding calmodulin in familial idiopathic ventricular fibrillation in childhood and adolescence. *J Am Coll Cardiol* **63**, 259–266.

29 Crotti L, Johnson CN, Graf E, De Ferrari GM, Cuneo BF, Ovadia M, Papagiannis J, Feldkamp MD, Rathi SG, Kunic JD, Pedrazzini M, Wieland T, Lichtner P, Beckmann B-M, Clark T, Shaffer C, Benson DW, Kääb S, Meitinger T, Strom TM, Chazin WJ, Schwartz PJ & George AL (2013) Calmodulin mutations associated with recurrent cardiac arrest in infants. *Circulation* **127**, 1009–1017.

30 Makita N, Yagihara N, Crotti L, Johnson CN, Beckmann BM, Roh MS, Shigemizu D, Lichtner P, Ishikawa T, Aiba T, Homfray T, Behr ER, Klug D, Denjoy I, Mastantuono E, Theisen D, Tsunoda T, Satake W, Toda T, Nakagawa H, Tsuji Y, Tsuchiya T, Yamamoto H, Miyamoto Y, Endo N, Kimura A, Ozaki K, Motomura H, Suda K, Tanaka T, Schwartz PJ, Meitinger T, Kaab S, Guicheney P, Shimizu W, Bhuiyan ZA, Watanabe H, Chazin WJ & George AL (2014) Novel Calmodulin Mutations Associated With Congenital Arrhythmia Susceptibility. *Circulation: Cardiovascular Genetics* **7**, 466–474.

31 Gomez-Hurtado N, Boczek NJ, Kryshtal DO, Johnson CN, Sun J, Nitu FR, Cornea RL, Chazin WJ, Calvert ML, Tester DJ, Ackerman MJ & Knollmann BC (2016) Novel CPVT-Associated Calmodulin Mutation in CALM3 (CALM3-A103V) Activates Arrhythmogenic Ca Waves and Sparks. *Circ Arrhythm Electrophysiol* **9**, 2510.

32 Boczek NJ, Gomez-Hurtado N, Ye D, Calvert ML, Tester DJ, Kryshtal DO, Hwang H-S, Johnson CN, Chazin WJ, Loporcaro CG, Shah M, Papez AL, Lau YR, Kanter R, Knollmann BC & Ackerman MJ (2016) Spectrum and Prevalence of CALM1-, CALM2-, and CALM3-Encoded Calmodulin Variants in Long QT Syndrome and Functional Characterization of a Novel Long QT Syndrome-Associated Calmodulin Missense Variant, E141G. *Circulation: Cardiovascular Genetics* **9**, 136–146.

33 Reed GJ, Boczek NJ, Etheridge SP & Ackerman MJ (2015) CALM3 mutation associated with long QT syndrome. *Heart Rhythm* **12**, 419–422.

34 Yin G, Hassan F, Haroun AR, Murphy LL, Crotti L, Schwartz PJ, George AL & Satin J (2014) Arrhythmogenic calmodulin mutations disrupt intracellular cardiomyocyte Ca^{2+} regulation by distinct mechanisms. *J Am Heart Assoc* **3**, e000996.

35 Pipilas DC, Johnson CN, Webster G, Schlaepfer J, Fellmann F, Sekarski N, Wren LM, Ogorodnik KV, Chazin DM, Chazin WJ, Crotti L, Bhuiyan ZA & George AL (2016) Novel calmodulin mutations associated with congenital long qt syndrome affect calcium current in human cardiomyocytes. *Heart Rhythm*.

36 Rocchetti M, Sala L, Dreizehnter L, Crotti L, Sinnecker D, Mura M, Pane LS, Altomare C, Torre E, Mostacciuolo G, Severi S, Porta A, De Ferrari GM, George AL, Schwartz PJ, Gnecchi M, Moretti A & Zaza A (2017) Elucidating arrhythmogenic mechanisms of long-QT syndrome CALM1-F142L mutation in patient-specific induced pluripotent stem cell-derived cardiomyocytes. *Cardiovasc Res* **113**, 531–541.

37 Wang K, Holt C, Lu J, Brohus M, Larsen KT, Overgaard MT, Wimmer R & Van Petegem F (2018) Arrhythmia mutations in calmodulin cause conformational changes that affect interactions with the cardiac voltage-gated calcium channel. *Proc Natl Acad Sci USA* **8**, 201808733.

38 Søndergaard MT, Sorensen AB, Skov LL, Kjaer-Sorensen K, Bauer MC, Nyegaard M, Linse S, Oxvig C & Overgaard MT (2015) Calmodulin mutations causing catecholaminergic polymorphic ventricular tachycardia confer opposing functional and biophysical molecular changes. *FEBS J.* **282**, 803–816.

39 Søndergaard MT, Liu Y, Brohus M, Guo W, Nani A, Carvajal C, Fill M, Overgaard MT & Chen SRW (2019) Diminished inhibition and facilitated activation of RyR2-mediated Ca^{2+} release is a common defect of arrhythmogenic calmodulin mutations. *FEBS J.* **286**, 4554–4578.

40 Vassilakopoulou V, Calver BL, Thanassoulas A, Beck K, Hu H, Buntwal L, Smith A, Theodoridou M, Kashir J, Blayney L, Livaniou E, Nounesis G, Anthony Lai F & Nomikos M (2015) Distinctive malfunctions of calmodulin mutations associated with heart RyR2-mediated arrhythmic disease. *Biochim Biophys Acta*.

41 Jones PP, Jiang D, Bolstad J, Hunt DJ, Zhang L, Demaurex N & Chen SRW (2008) Endoplasmic reticulum Ca^{2+} measurements reveal that the cardiac ryanodine receptor mutations linked to cardiac arrhythmia and sudden death alter the threshold for store-overload-induced Ca2+ release. *Biochem. J.* **412**, 171–178.

42 Yamniuk AP & Vogel HJ (2004) Calmodulin's flexibility allows for promiscuity in its interactions with target proteins and peptides. *Mol. Biotechnol.* **27**, 33–57.

43 Yap KL, Kim J, Truong K, Sherman M, Yuan T & Ikura M (2000) Calmodulin target database. *J. Struct. Funct. Genomics* **1**, 8–14.

44 Zhang J, Liu Z, Masumiya H, Wang R, Jiang D, Li F, Wagenknecht T & Chen SRW (2003) Three-dimensional localization of divergent region 3 of the ryanodine receptor to the clamp-shaped structures adjacent to the FKBP binding sites. *Journal of Biological Chemistry* **278**, 14211–14218.

45 Rhoads AR & Friedberg F (1997) Sequence motifs for calmodulin recognition. *FASEB J.* **11**, 331–340.

46 Brohus M, Søndergaard MT, Wayne Chen SR, Van Petegem F & Overgaard MT (2019) Ca^{2+}-dependent calmodulin binding to cardiac ryanodine receptor (RyR2) calmodulin-binding domains. *Biochem. J.* **476**, 193–209.

47 Ngo VA, Perissinotti LL, Miranda W, Chen SRW & Noskov SY (2017) Mapping Ryanodine Binding Sites in the Pore Cavity of Ryanodine Receptors. *Biophys J* **112**, 1645–1653.

48 Du GG, Imredy JP & MacLennan DH (1998) Characterization of recombinant rabbit cardiac and skeletal muscle Ca^{2+} release channels (ryanodine receptors) with a novel [3H]ryanodine binding assay. *Journal of Biological Chemistry* **273**, 33259–33266.

49 Breitwieser GE & Gama L (2001) Calcium-sensing receptor activation induces intracellular calcium oscillations. *Am. J. Physiol., Cell Physiol.* **280**, C1412–21.

50 Jiang D, Xiao B, Yang D, Wang R, Choi P, Zhang L, Cheng H & Chen SRW (2004) RyR2 mutations linked to ventricular tachycardia and sudden death reduce the threshold for store-overload-induced Ca^{2+} release (SOICR). *Proc Natl Acad Sci USA* **101**, 13062–13067.

51 Xiao Z, Guo W, Sun B, Hunt DJ, Wei J, Liu Y, Wang Y, Wang R, Jones PP, Back TG & Chen SRW (2016) Enhanced Cytosolic Ca^{2+} Activation Underlies a Common Defect of Central Domain Cardiac Ryanodine Receptor Mutations Linked to Arrhythmias. *J Biol Chem* **291**, 24528–24537.

52 Liu Y, Sun B, Xiao Z, Wang R, Guo W, Zhang JZ, Mi T, Wang Y, Jones PP, Van Petegem F & Chen SRW (2015) Roles of the NH2-terminal Domains of Cardiac Ryanodine Receptor in Ca^{2+} Release Activation and Termination. *J Biol Chem* **290**, 7736–7746.

53 Jensen HH, Brohus M, Nyegaard M & Overgaard MT (2018) Human Calmodulin Mutations. *Front Mol Neurosci* **11**, 396.

54 Nomikos M, Thanassoulas A, Beck K, Vassilakopoulou V, Hu H, Calver BL, Theodoridou M, Kashir J, Blayney L, Livaniou E, Rizkallah P, Nounesis G & Lai FA (2014) Altered RyR2 regulation by the calmodulin F90L mutation associated with idiopathic ventricular fibrillation and early sudden cardiac death. *FEBS Lett* **588**, 2898–2902.

55 Ono M, Yano M, Hino A, Suetomi T, Xu X, Susa T, Uchinoumi H, Tateishi H, Oda T, Okuda S, Doi M, Kobayashi S, Yamamoto T, Koseki N, Kyushiki H, Ikemoto N & Matsuzaki M (2010) Dissociation of

calmodulin from cardiac ryanodine receptor causes aberrant Ca(2+) release in heart failure. *Cardiovasc Res* **87**, 609–617.

56 Rodney GG, Krol J, Williams B, Beckingham K & Hamilton SL (2001) The carboxy-terminal calcium binding sites of calmodulin control calmodulin's switch from an activator to an inhibitor of RYR1. *Biochemistry* **40**, 12430–12435.

57 Walweel K, Gomez-Hurtado N, Oo YW, Beard NA, Remedios Dos C, Johnson CN, Chazin WJ, van Helden DF, Knollmann BC & Laver DR (2017) Calmodulin Mutants Linked to Catecholaminergic Polymorphic Ventricular Tachycardia Fail to Inhibit Human RyR2 Channels. *J Am Coll Cardiol* **70**, 115–117.

58 Chen W, Wang R, Chen B, Zhong X, Kong H, Bai Y, Zhou Q, Xie C, Zhang J, Guo A, Tian X, Jones PP, O'Mara ML, Liu Y, Mi T, Zhang L, Bolstad J, Semeniuk L, Cheng H, Zhang J, Chen J, Tieleman DP, Gillis AM, Duff HJ, Fill M, Song L-S & Chen SRW (2014) The ryanodine receptor store-sensing gate controls Ca(2+) waves and Ca(2+)-triggered arrhythmias. **20**, 184–192.

59 Tang Y, Tian X, Wang R, Fill M & Chen SRW (2012) Abnormal termination of Ca^{2+} release is a common defect of RyR2 mutations associated with cardiomyopathies. *Circ Res* **110**, 968–977.

60 Zhou Q, Xiao J, Jiang D, Wang R, Vembaiyan K, Wang A, Smith CD, Xie C, Chen W, Zhang J, Tian X, Jones PP, Zhong X, Guo A, Chen H, Zhang L, Zhu W, Yang D, Li X, Chen J, Gillis AM, Duff HJ, Cheng H, Feldman AM, Song L-S, Fill M, Back TG & Chen SRW (2011) Carvedilol and its new analogs suppress arrhythmogenic store overload-induced Ca^{2+} release. **17**, 1003–1009.

61 Priori SG & Chen SRW (2011) Inherited dysfunction of sarcoplasmic reticulum Ca2+ handling and arrhythmogenesis. *Circ Res* **108**, 871–883.

62 Jiang D, Wang R, Xiao B, Kong H, Hunt DJ, Choi P, Zhang L & Chen SRW (2005) Enhanced store overload-induced Ca^{2+} release and channel sensitivity to luminal Ca2+ activation are common defects of RyR2 mutations linked to ventricular tachycardia and sudden death. *Circ Res* **97**, 1173–1181.

63 Larkin MA, Blackshields G, Brown NP, Chenna R, McGettigan PA, McWilliam H, Valentin F, Wallace IM, Wilm A, Lopez R, Thompson JD, Gibson TJ & Higgins DG (2007) Clustal W and Clustal X version 2.0. *Bioinformatics* **23**, 2947–2948.

64 Chen SR & MacLennan DH (1994) Identification of calmodulin-, Ca^{2+}-, and ruthenium red-binding domains in the Ca^{2+} release channel (ryanodine receptor) of rabbit skeletal muscle sarcoplasmic reticulum. *Journal of Biological Chemistry* **269**, 22698–22704.

65 Zhang H, Zhang J-Z, Danila CI & Hamilton SL (2003) A noncontiguous, intersubunit binding site for calmodulin on the skeletal muscle Ca^{2+} release channel. *Journal of Biological Chemistry* **278**, 8348–8355.

66 Palmer AE, Jin C, Reed JC & Tsien RY (2004) Bcl-2-mediated alterations in endoplasmic reticulum Ca^{2+} analyzed with an improved genetically encoded fluorescent sensor. *Proc Natl Acad Sci USA* **101**, 17404–17409.

67 Zhao M, Li P, Li X, Zhang L, Winkfein RJ & Chen SR (1999) Molecular identification of the ryanodine receptor pore-forming segment. *Journal of Biological Chemistry* **274**, 25971–25974.

68 Ho SN, Hunt HD, Horton RM, Pullen JK & Pease LR (1989) Site-directed mutagenesis by overlap extension using the polymerase chain reaction. *Gene* **77**, 51–59.

69 Zhao M, Li P, Li X, Zhang L, Winkfein RJ & Chen SR (1999) Molecular identification of the ryanodine receptor pore-forming segment. *Journal of Biological Chemistry* **274**, 25971–25974.

70 Dweck D, Reyes-Alfonso A & Potter JD (2005) Expanding the range of free calcium regulation in biological solutions. *Anal Biochem* **347**, 303–315.

71 Guo W, Sun B, Xiao Z, Liu Y, Wang Y, Zhang L, Wang R & Chen SRW (2015) The EF-hand Ca^{2+} Binding Domain Is Not Required for Cytosolic Ca^{2+} Activation of the Cardiac Ryanodine Receptor. *J Biol Chem*, jbc.M115.693325.

72 Schneider CA, Rasband WS & Eliceiri KW (2012) NIH Image to ImageJ: 25 years of image analysis. *Nat. Methods* **9**, 671–675.

73 Xiao B, Jiang MT, Zhao M, Yang D, Sutherland C, Lai FA, Walsh MP, Warltier DC, Cheng H & Chen SRW (2005) Characterization of a novel PKA phosphorylation site, serine-2030, reveals no PKA hyperphosphorylation of the cardiac ryanodine receptor in canine heart failure. *Circ Res* **96**, 847–855.

TABLES

Table 1: RyR2 CaM-binding domains investigated and RyR2 variants used in this study. Amino acid numbering corresponds to human RyR2 (UniprotKB **Q92736**) where nothing else is mentioned. RyR2 mutations were introduced in the mouse RyR2 cDNA and transfected into HEK293 Flp-In cells. The human and mouse RyR2 proteins differ minutely such that human RyR2 CaMBD numbering corresponds to mouse RyR2 numbering +1. See alignment in Figure 2.

CaMBD	Residues	RyR2 mutation (murine)	RyR2 variant	Comments	References
CaMBD1a	F1942 - R1966	ΔF1941-T1961	RyR2-ΔCaMBD1a	Extrapolated from apoCaM binding to RyR1	[15,46,65]
CaMBD1b	L2029 - S2056	ΔL2028-A2048	RyR2-ΔCaMBD1b	Encompasses the S2031 phosphorylation site and a putative CaM binding motif	[46,64,73]
CaMBD2	R3581 - P3607	ΔK3582-F3602	RyR2-ΔCaMBD2	Well-established and pivotal for CaM-RyR2 interaction	[5,15,17,46]
CaMBD3	F4246 - V4276	ΔF4245-K4265	RyR2-ΔCaMBD3	CaM's affinity for CaMBD2 and -3 are similar at the peptide level	[15,46]

Table 2: RyR2 CaMBD peptides used in this study. Numbering corresponds to human RyR2 (UniprotKB Q92736).

Nomenclature	RyR2 Residues	Peptide Sequence (Length)	Ref
CaMBD1a	R1941 - F1965	RFRYNEVMQALNMSAALTARKTKEF (25)	[15,46,65]
CaMBD1b	D2022 - S2052	DLTIRGRLLSLVEKVTYLKKKQAEKPVESDS (31)	[46,64,73]
CaMBD2	R3581 - L3611	RSKKAVWHKLLSKQRKRAVVACFRMAPLYNL (31)	[8,16,25,46]
CaMBD3	F4246 - V4276	FALRYNILTLMRMLSLKSLKKQMKKVKKMTV (31)	[15,46]

Table 3: Fitted dissociation constants from CaM titrations of RyR2 CaMBD1a and CaMBD1b peptides. $\Delta\Delta G^o$ and data are only shown for $[Ca^{2+}]_{free}$ were K_D or K_{DI} values were significantly different for CaM-N54I compared to CaM-WT. K_D, K_{DI} and $[Ca^{2+}]_{free}$ are given in μM, and $\Delta\Delta G^o$ in kJ/mol.

K_{DI} for binding to CaMBD**1a**	K_D for binding to CaMBD**1b**

$[Ca^{2+}]_{free}$	CaM-WT	CaM-N54I	$\Delta\Delta G^o$	CaM-WT	CaM-N54I	$\Delta\Delta G^o$
2	1.51	1.88	0.5	0.33	0.44	0.7
4	0.64	0.90	0.9	0.14	0.21	1.1
10	0.27	0.43	1.1	0.07	0.12	1.6
25	0.14	0.21	1.1	0.04	0.08	1.8
100	0.10	0.13	0.7	0.02	0.06	2.0
398	0.08	0.11	0.6	0.03	0.05	1.6

Table 4: Quantified Ca^{2+} release properties for RyR2 variants investigated in intact HEK293 cells. Activation and termination thresholds as well as fractional ER Ca^{2+} release are given in units of % with SD in parentheses (see Figure 5).

RyR2 variant / CaM plasmid expression	Activation Threshold	Termination Threshold	Fractional Ca^{2+} Release	Analysed Traces
RyR2 WT	89 (4.7)	58 (5.2)	31 (5.4)	108
RyR2 WT + CaM	90 (4.2)	62 (5.9)	29 (5.2)	50
RyR2 WT + CaM-N54I	85 (6.3)	49 (5.2)	36 (6.7)	47
RyR2-ΔCaMBD1a	98 (3.2)	36 (7.3)	61 (6.9)	55
RyR2-ΔCaMBD1a + CaM	100 (2.0)	57 (5.8)	44 (6.9)	4
RyR2-ΔCaMBD1a + CaM-N54I	97 (2.8)	42 (7.1)	55 (7.6)	23
RyR2-ΔCaMBD1b	83 (6.6)	58 (7.2)	25 (4.8)	93
RyR2-ΔCaMBD1b + CaM	85 (4.5)	63 (5.7)	22 (3.8)	32
RyR2-ΔCaMBD1b + CaM-N54I	83 (4.0)	53 (6.7)	31 (5.9)	25
RyR2-ΔCaMBD2	93 (3.2)	35 (6.1)	57 (7.4)	69
RyR2-ΔCaMBD3	88 (4.7)	58 (7.0)	30 (6.3)	57
RyR2-ΔCaMBD3 + CaM	91 (5.2)	64 (4.2)	27 (4.3)	22
RyR2-ΔCaMBD3 + CaM-N54I	87 (6.3)	49 (7.2)	38 (6.5)	37

Table 5: Steady-state ER Ca^{2+} load in permeabilized HEK293 cells expressing RyR2 variants, and with 1 μM cytosolic side $[Ca^{2+}]_{free}$. The steady-state ER Ca^{2+} load without CaM or with CaM-WT or -N54I added to perfusion medium are listed. ER Ca^{2+} load and the effect of CaM are given in units of % with SD in parentheses (see Figure 8). Also provided are the number of analysed microscope cover slips with cells (slips) and the corresponding number of single cell traces (traces) analysed.

		RyR2-WT	**RyR2-ΔCaMBD1a**	**RyR2-ΔCaMBD1b**	**RyR2-ΔCaMBD2**	**RyR2-ΔCaMBD3**
Steady-state ER Ca^{2+} load	no CaM	32 (9.9)	31 (12)	31 (9.4)	33 (11)	30 (7.7)
	+ CaM-WT	41 (12)	54 (15)	39 (10)	34 (11)	39 (8.6)
	+ CaM-N54I	27 (7.1)	41 (13)	25 (4.5)	n/a	23 (6.2)
Effect of CaM	CaM-WT	9.1 (4.6)	21 (8.0)	6.5 (5.1)	1 (2.8)	7.9 (4.2)
	CaM-N54I	-3.7 (2.6)	15 (8.4)	-4.3 (2.3)	n/a	-4.3 (4.1)
Slips / traces	using CaM-WT	10 / 197	11 / 126	7 / 163	4 / 82	5 / 85
	using CaM-N54I	4 / 66	5 / 56	3 / 46	n/a	7 / 150

FIGURE LEGENDS

Figure 1: **Locations of CaM and RyR2 CaMBDs on the homotetrameric RyR2 channel**. Structural details from two cryo-EM structures of the RyR2-CaM complex under different Ca^{2+} conditions are shown. Three RyR2 monomers are semi-transparent to emphasise the one inspected closer. Left: Images of a RyR2-CaM structure also containing peptidyl-prolyl cis-trans isomerase FKBP1B (FKBP12.6) and obtained in the absence of Ca^{2+} (PDB file **6JI8**). Right: Images from a RyR2-CaM structure obtained in the presence of Ca^{2+} (PDB file **6JV2**). The RyR2 channel is shown in side-view with a smaller top-view inserted (A-B), and for each structure a zoom on the CaM-binding region is shown in two representations: C-D) Close-up view of CaM bound to RyR2 in surface representation, and E-F) detailed view further zoomed in and with details in protein secondary structure representation. Amino acids part of RyR2 CaMBD1a, -1b and 2 are colour-highlighted, and so are the amino acids nearest to CaMBD3 (colour legend in figure). The CaM N-domain is shown in blue and the C-domain in orange throughout. Methionine residues part of the CaM N-domain's binding groove are highlighted in white. Note that Asn-54 (highlighted as red dots in E-F) is not buried in RyR2 in either CaM conformation. RyR2 Phe-3603 and Trp-3587 are highlighted as green stick models. Rotation axis indicate structure translocation from top views to side views (inserts to A-B), and from side-views to zoomed views of CaM (A-B to C-F).

Figure 2: **RyR sequence alignment for regions around CaMBDs**. Partial alignment shown for human RyR (hRyR1-3) and mouse RyR2 (mRyR2). The protein sequence alignment was made using ClustalW and 15 RyR sequences from human, mouse, rabbit, chicken, zebrafish, *C. elegans*, *D. melanogaster* and *O. dioica* [63]. UniprotKB files **P21817**, **Q92736**, **Q15413**, **E9PZQ0**, **E9Q401**, **A2AGL3**, **P11716**, **P30957**, **Q9TS33**, **F1NLZ9**, **Q90985**, **A6P4B8**, **P91905**, **Q24498**, **E4XPI8**. Bars reflect the degree of conservation across all 15 aligned RyR sequences. Investigated RyR2 CaMBDs are highlighted in yellow, and the residues deleted in the murine RyR2-ΔCaMBD variants are underlined in red. CaM-binding motifs, identified by searches using the calmodulin target database, are lined above in grey.

Figure 3: **Ca^{2+}-dependent affinities of CaM-WT and -N54I for binding to RyR2 CaMBD peptides**. The dissociation constants for the binding of CaM to peptides (K_D, or K_{DI} for RyR2 CaMBD1a titrations) are plotted for discrete $[Ca^{2+}]_{free}$. Dashed, connecting lines are added to ease overview only. Note the double logarithmic axes. Asterisks indicate significant differences in K_D or K_{DI} between CaM-WT and -N54I for binding to CaMBD1a and CaMBD1b peptides, also summarized in Table 3 (unpaired t-tests with Holm-Sidak

correction, $p < 0.05$). There were no significant differences between CaM-WT and -N54I in the fitted K_D for their affinity for binding to RyR2 CaMBD2 and nor for their binding to CaMBD3.

Figure 4: **[^{3}H]ryanodine binding to RyR2 variants at 1 μM [Ca^{2+}]$_{free}$. A**) Cell lysates from HEK293 expressing RyR2 variants were incubated with [^{3}H]ryanodine and without (black), with purified CaM-N54I (tangerine) or with CaM-WT (grey). The extent of [^{3}H]ryanodine binding to RyR2 was quantified using scintillation counting and normalized to lysate protein concentration (0.5-0.8 g/L) such that y-axis units are counts·L·h^{-1}·g^{-1}. Solid lines show fits to a one-phase association model. Note the different y-axis ranges in each panel. **B**) Estimation of the extent of [^{3}H]ryanodine binding to RyR2 at the reaction equilibrium (B_{eq}, see 'Materials and methods'). Comparisons were made for the reactions without CaM added, and asterisk indicate values significantly different from the B_{eq} for RyR2-WT (1-way ANOVA with Holm-Sidak correction, $p < 0.05$). **C**) Effects of CaM on the association rate of [^{3}H]ryanodine to each RyR2 variant. Asterisks indicate an association rate significantly different from that of the reaction without CaM added (1-way ANOVA with Holm-Sidak correction, $p < 0.05$). Error bars show the sample standard deviation (SD) in all panels and four replicates were made for each reaction.

Figure 5: **Store overload-induced Ca^{2+} release in RyR2-expressing HEK293 cells**. Example time traces for the FRET signal from the ER luminal D1ER Ca^{2+} probe, oscillating with RyR2 Ca^{2+} releases. FRET is measured as the ratio of yellow to cyan D1ER protein fluorescence (YFP/CFP). Concentrations of Ca^{2+}, tetracaine and caffeine in the perfusion solution are shown in rectangles. Increasing extracellular Ca^{2+} concentration elicited RyR2 SOICR oscillations, tetracaine blocked Ca^{2+} release thereby filling ER to maximum ER Ca^{2+} load, and caffeine opened RyR2 channels depleting ER Ca^{2+}. Tetracaine and caffeine were used to establish FRET signals for maximum and minimum ER Ca^{2+} load (F_{max} and F_{min}), respectively. The activation and termination thresholds, and the fractional ER Ca^{2+} release were calculated relative to F_{max} and F_{min}. One example FRET trace is shown for single cells expressing either RyR2, -ΔCaMBD1a, -ΔCaMBD1b or -ΔCaMBD3, and all with CaM-WT plasmid expression. The full data set from the individual analysis of hundreds of such single cell traces is shown in Figure 6 and Table 4.

Figure 6: **Ca^{2+} release properties of RyR2 and CaMBD deletion variants during SOICR**. Plots show the activation threshold (**A**), termination threshold (**B**) and fractional ER Ca^{2+} release (**C**) averaged from multiple traces (means with 95 % confidence interval (CI)). For each RyR2 variant, three conditions of CaM expression were assayed: endogenous CaM (control), and CaM or CaM-N54I transient expression. RyR2-ΔCaMBD2 does

not respond to CaM expression condition, hence only one condition. For each RyR2 variant, asterisk (*) indicates significant differences between the condition with CaM-WT expression and endogenous or CaM-N54I expression (1-way ANOVA with Dunnett's correction, $p < 0.05$). Plus (+) indicates significant differences between the RyR2-WT and each RyR2 CaMBD deletion variant given the same CaM expression condition (1-way ANOVA with Dunnett's correction, $p < 0.05$). Measured values and number of replicates are summarized in Table 4.

Figure 7: **RyR2 Ca^{2+} release in permeabilized RyR2-expressing HEK293 cells**. Example D1ER FRET signal from permeabilized cells (3-5 averaged) perfused with sustained, cytosolic side Ca^{2+}. ΔYFP/CFP is the difference between the D1ER FRET minimum signal (F_{min}) and the FRET signal at each time point (baseline subtraction). Five different cell lines (**A-E**) expressing either RyR2-WT, -ΔCaMBD1a, -ΔCaMBD1b, -ΔCaMBD2 or -ΔCaMBD3 were used with either CaM-WT (grey) or CaM-N54I (tangerine) addition. The continuous ER Ca^{2+} release (RyR2) and Ca^{2+} uptake (SERCA2b) establishes a steady-state ER Ca^{2+} load during each perfusion condition (labelled rectangles). Tetracaine (1 mM) and caffeine (20 mM) were used to establish FRET signals for maximum and minimum ER Ca^{2+} load (F_{max} and F_{min}). Steady-state ER Ca^{2+} load at 1 μM $[Ca^{2+}]_{free}$ was the average FRET signal, relative to $F_{max} – F_{min}$, during perfusion without ($F_{1.0}$) and with CaM added ($F_{CaM\text{-}WT}$ or $F_{CaM\text{-}N54I}$). The differences $F_{CaM\text{-}WT} - F_{1.0}$ or $F_{CaM\text{-}N54I} - F_{1.0}$ quantify the effects on steady-state ER Ca^{2+} load from adding CaM-WT or -N54I. RyR2-ΔCaMBD2 is insensitive to regulation by CaM and was included as a control and therefore only perfused with CaM-WT. The traces shown are examples of the type of experiment data obtained, and the full data set from the individual analysis of hundreds of such single cell traces is shown in Figure 8 and Table 5.

Figure 8: **Measured steady-state ER Ca^{2+} load in the presence of sustained 1 μM cytosolic Ca^{2+} in permeabilized HEK293 cells expressing RyR2 variants**. **A**) Plot of the measured steady-state ER Ca^{2+} loads before (no CaM, green) and after the addition of purified CaM-WT (grey) or CaM-N54I (tangerine). **B**) The quantified effects of adding CaM-WT or CaM-N54I to permeabilized cells measured as the change in steady-state ER Ca^{2+} load compared to the condition without CaM. Note that percent is used as the unit for ER Ca^{2+} load and not as a measure of relative change (see 'Materials and methods'). For both A and B, lower case letters (a, b, c or d) indicate groups of averages significantly different from all other groups while asterisk (*) indicates a value distinct from all others except for the effect of CaM-WT on RyR2-WT (Kruskal-Wallis test with Dunn's correction, $p < 0.05$). Error bars correspond to the 95 % CI, and mean values and number of replicates are summarized in Table 5.

Figure 9: **Caffeine stimulated RyR2-mediated Ca^{2+} release in HEK293 cell suspensions**. **A**) Cells expressing RyR2 variants were loaded with a cytosolic Ca^{2+} indicator (Fluo-3), and each caffeine addition caused a transient increase in fluorescence (a peak). Example time traces are shown as normalized Fluo-3 fluorescence ($\Delta F/F_0$) as a function of the cumulative caffeine concentration. **B**) RyR2 Ca^{2+} release profiles quantified from time traces. Data points represent the normalized peak heights for each caffeine addition (see 'Materials and methods'). Solid lines are biphasic Hill fits for overview purposes only. Error bars show standard error of the mean from at least triplicate measurements. Filled-in symbols indicate points significantly different from the response of RyR2-WT (2-way ANOVA with Dunnett's correction, $p < 0.05$). The RyR2-ΔCaMBD1a and RyR2-ΔCaMD1b differed significantly from that of RyR2-WT at six out of eight cumulative caffeine concentrations.

Figure 10: **Estimation of CaM expression levels in HEK293 cells. A)** HEK293 cell lysates were Western-blotted for CaM and β-actin with bands visualized using chemiluminescence imaging. HEK293 cells were cultured without (Ctrl) and with plasmid expression of either CaM-WT or CaM-N54I (samples loaded left to right, and experiment done in triplicate). **B)** Quantified CaM expression levels in HEK293 cells. Protein expression levels of CaM were normalized to that of β-actin, and plasmid expression of either CaM variant significantly increased total CaM protein levels, compared to the control. Error bars correspond to SD. a or b indicate groups of averages significantly different from all others (one-way ANOVA with Tukey's correction, $p < 0.05$). No significant difference in CaM protein levels were observed comparing plasmid expression of CaM-WT and CaM-N54I.

SUPPORTING INFORMATION

Supplemental_data_table_1.csv contains all data points used for analysing the experiment using SOICR in RyR2-expressing HEK293 cells during single cell ER Ca^{2+} imaging. Data was used to prepare Table 4 and Figure 6.

Supplemental_data_table_2.csv contains all data points used for analysing the experiment using permeabilised, RyR2-expressing HEK293 cells added purified CaM during single cell ER Ca^{2+} imaging. Data was used to prepare Table 5 and Figure 8.

ACKNOWLEDGEMENTS

(No acknowledgements to include. Funding sources have been listed in the submission system).

AUTHOR CONTRIBUTIONS

MTS, YL, WG, JW and MB performed experiments and analyzed the data. RW performed and validated the molecular cloning of RyR2 encoding plasmids. MTS, SRWC and MTO designed and directed the study. MTS and SRWC consolidated results across experiments, completed statistical analyses and wrote the manuscript.

CONFLICTS OF INTEREST

The authors declare not to have any actual or potential conflict of interest including any financial, personal or other relationships with other people or organizations within three years of beginning the submitted work that could inappropriately influence, or be perceived to influence, our work.

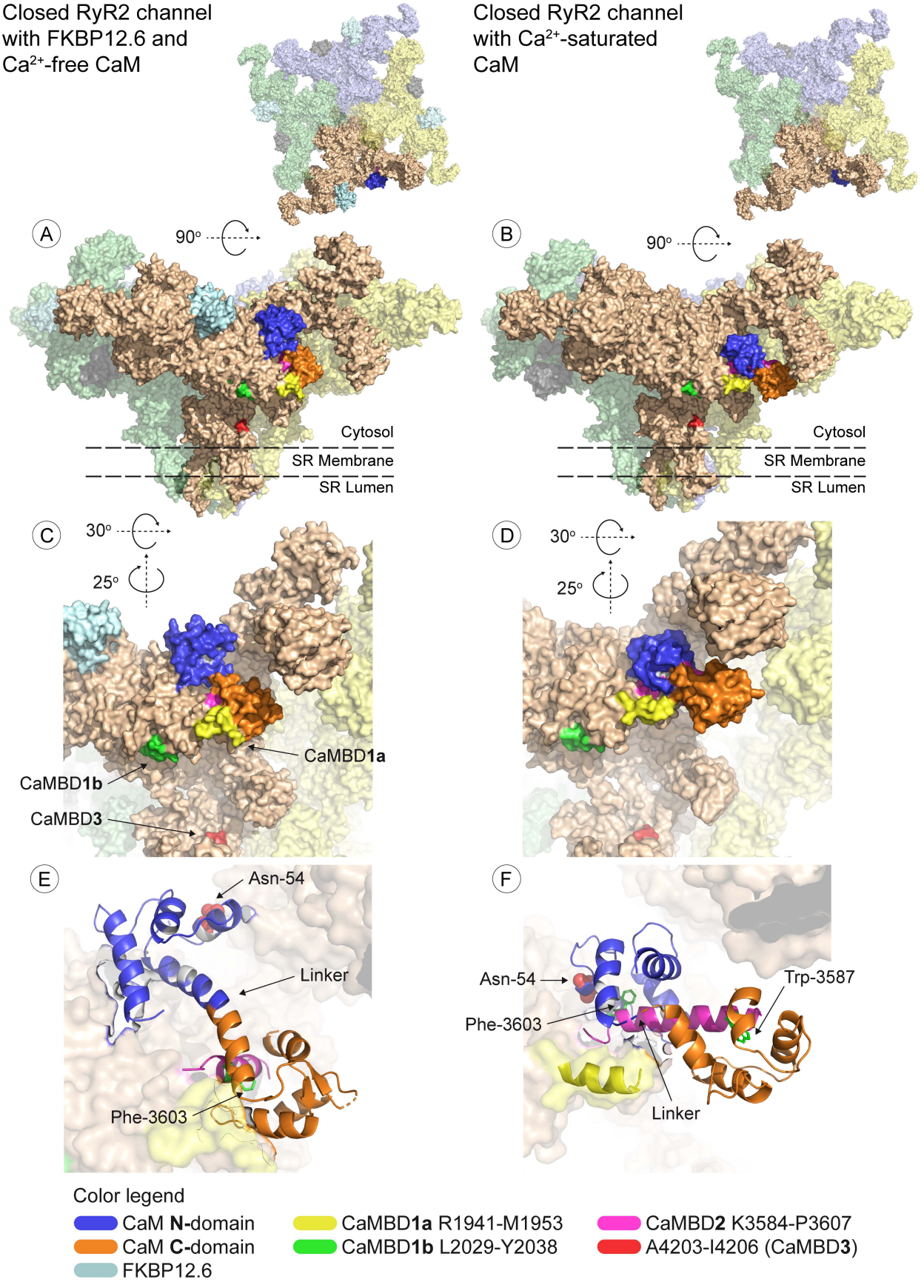
Closed RyR2 channel with FKBP12.6 and Ca2+-free CaM
Closed RyR2 channel with Ca2+-saturated CaM
A
B
90°
Cytosol
SR Membrane
SR Lumen
C
D
30°
25°
CaMBD1a
CaMBD1b
CaMBD3
E
F
Asn-54
Linker
Phe-3603
Trp-3587
Color legend
CaM N-domain
CaM C-domain
FKBP12.6
CaMBD1a R1941-M1953
CaMBD1b L2029-Y2038
CaMBD2 K3584-P3607
A4203-I4206 (CaMBD3)

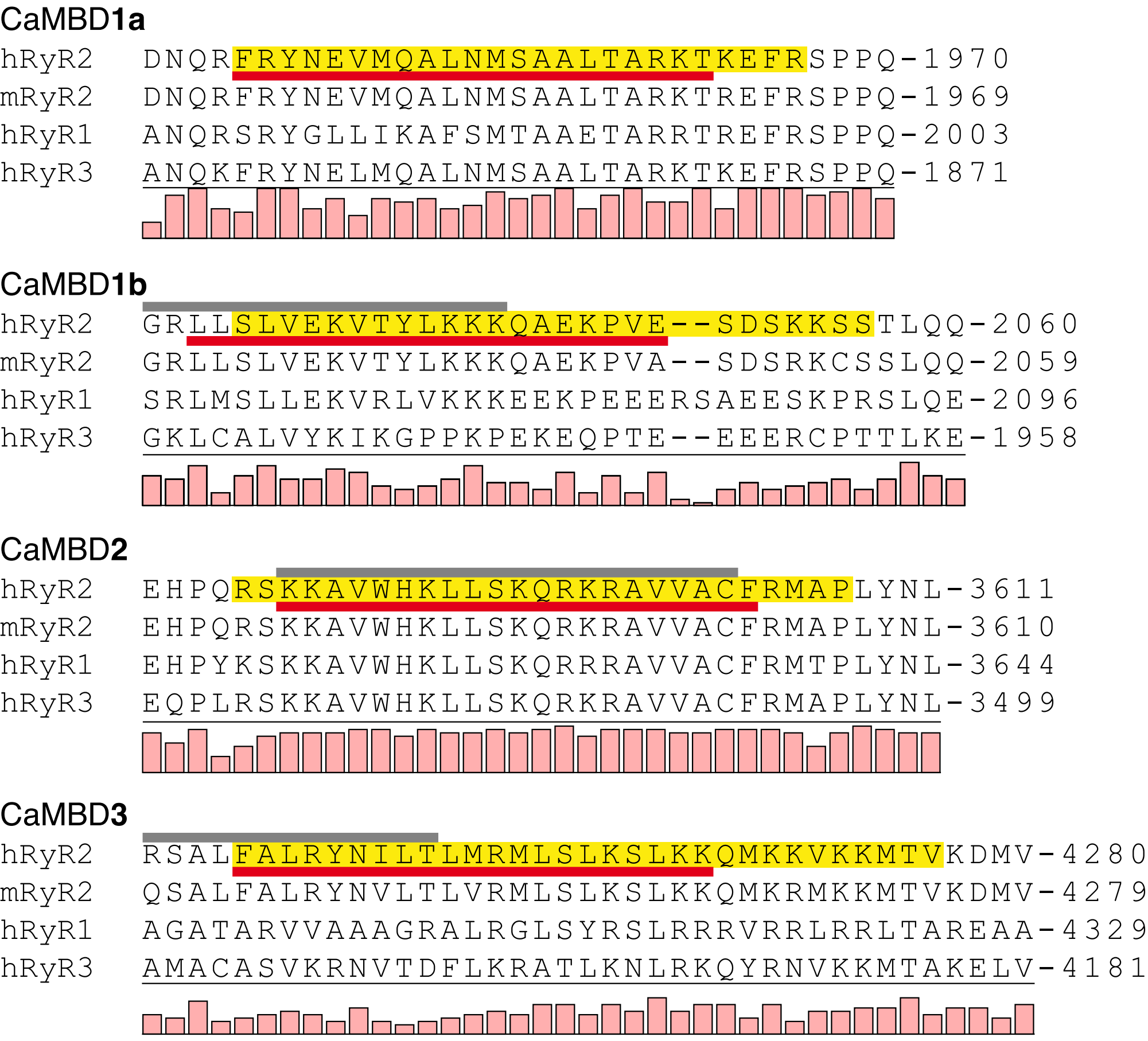
CaMBD1a
hRyR2 DNQRFRYNEVMQALNMSAALTARKTKEFRSPPQ-1970
mRyR2 DNQRFRYNEVMQALNMSAALTARKTREFRSPPQ-1969
hRyR1 ANQRSRYGLLIKAFSMTAAETARRTREFRSPPQ-2003
hRyR3 ANQKFRYNELMQALNMSAALTARKTKEFRSPPQ-1871
CaMBD1b
hRyR2 GRLLSLVEKVTYLKKKQAEKPVE--SDSKKSSTLQQ-2060
mRyR2 GRLLSLVEKVTYLKKKQAEKPVA--SDSRKCSSLQQ-2059
hRyR1 SRLMSLLEKVRLVKKKEEKPEEERSAEESKPRSLQE-2096
hRyR3 GKLCALVYKIKGPPKPEKEQPTE--EEERCPTTLKE-1958
CaMBD2
hRyR2 EHPQRSKKAVWHKLLSKQRKRAVVACFRMAPLYNL-3611
mRyR2 EHPQRSKKAVWHKLLSKQRKRAVVACFRMAPLYNL-3610
hRyR1 EHPYKSKKAVWHKLLSKQRRRAVVACFRMTPLYNL-3644
hRyR3 EQPLRSKKAVWHKLLSKQRKRAVVACFRMAPLYNL-3499
CaMBD3
hRyR2 RSALFALRYNILTLMRMLSLKSLKKQMKKVKKMTVKDMV-4280
mRyR2 QSALFALRYNVLTLVRMLSLKSLKKQMKRMKKMTVKDMV-4279
hRyR1 AGATARVVAAAGRALRGLSYRSLRRRVRRLRRLTAREAA-4329
hRyR3 AMACASVKRNVTDFLKRATLKNLRKQYRNVKKMTAKELV-4181

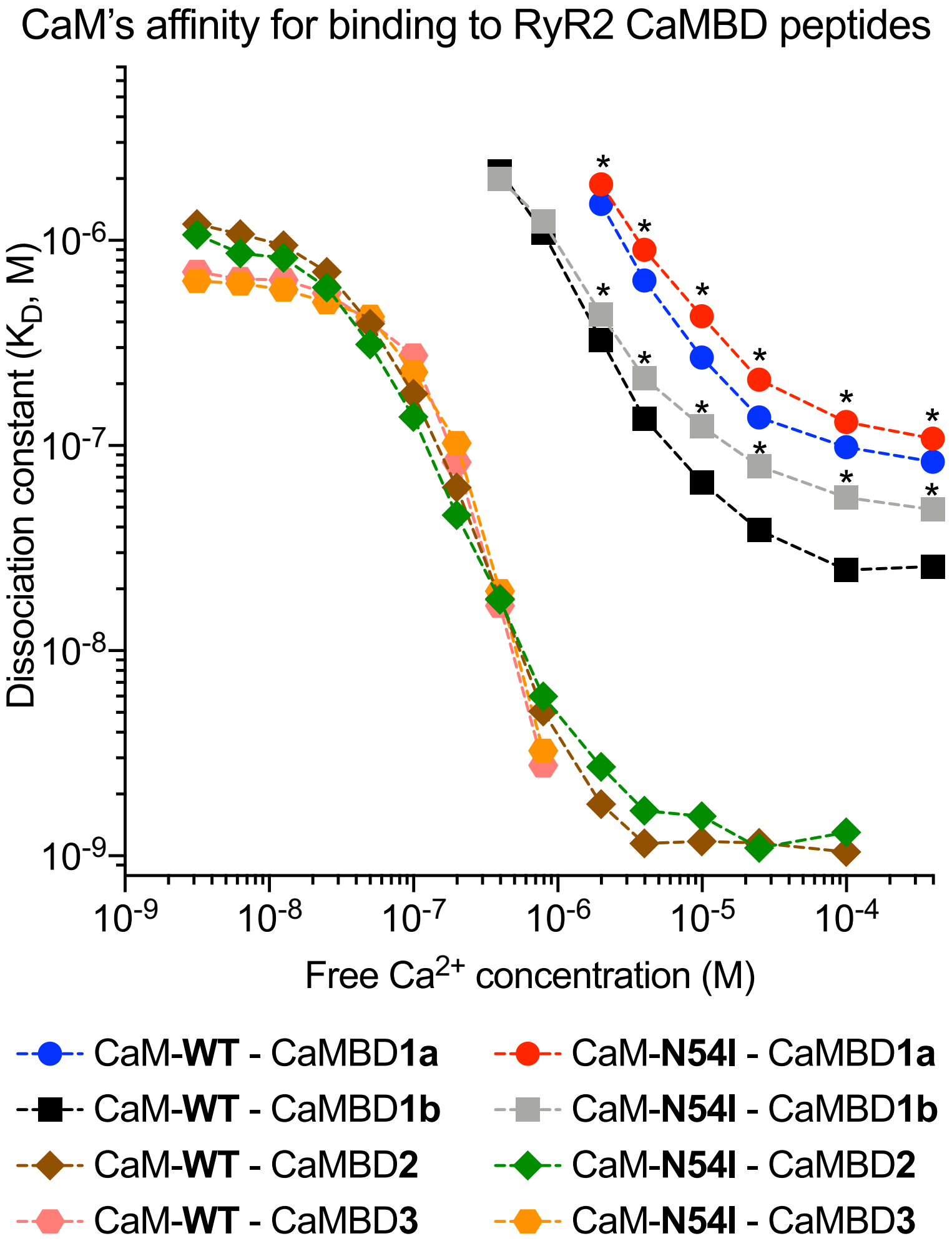
CaM's affinity for binding to RyR2 CaMBD peptides
Dissociation constant (K_D, M)
10^{-6}
10^{-7}
10^{-8}
10^{-9}
10^{-9}
10^{-8}
10^{-7}
10^{-6}
10^{-5}
10^{-4}
Free Ca^{2+} concentration (M)
CaM-**WT** - CaMBD**1a**
CaM-**N54I** - CaMBD**1a**
CaM-**WT** - CaMBD**1b**
CaM-**N54I** - CaMBD**1b**
CaM-**WT** - CaMBD**2**
CaM-**N54I** - CaMBD**2**
CaM-**WT** - CaMBD**3**
CaM-**N54I** - CaMBD**3**

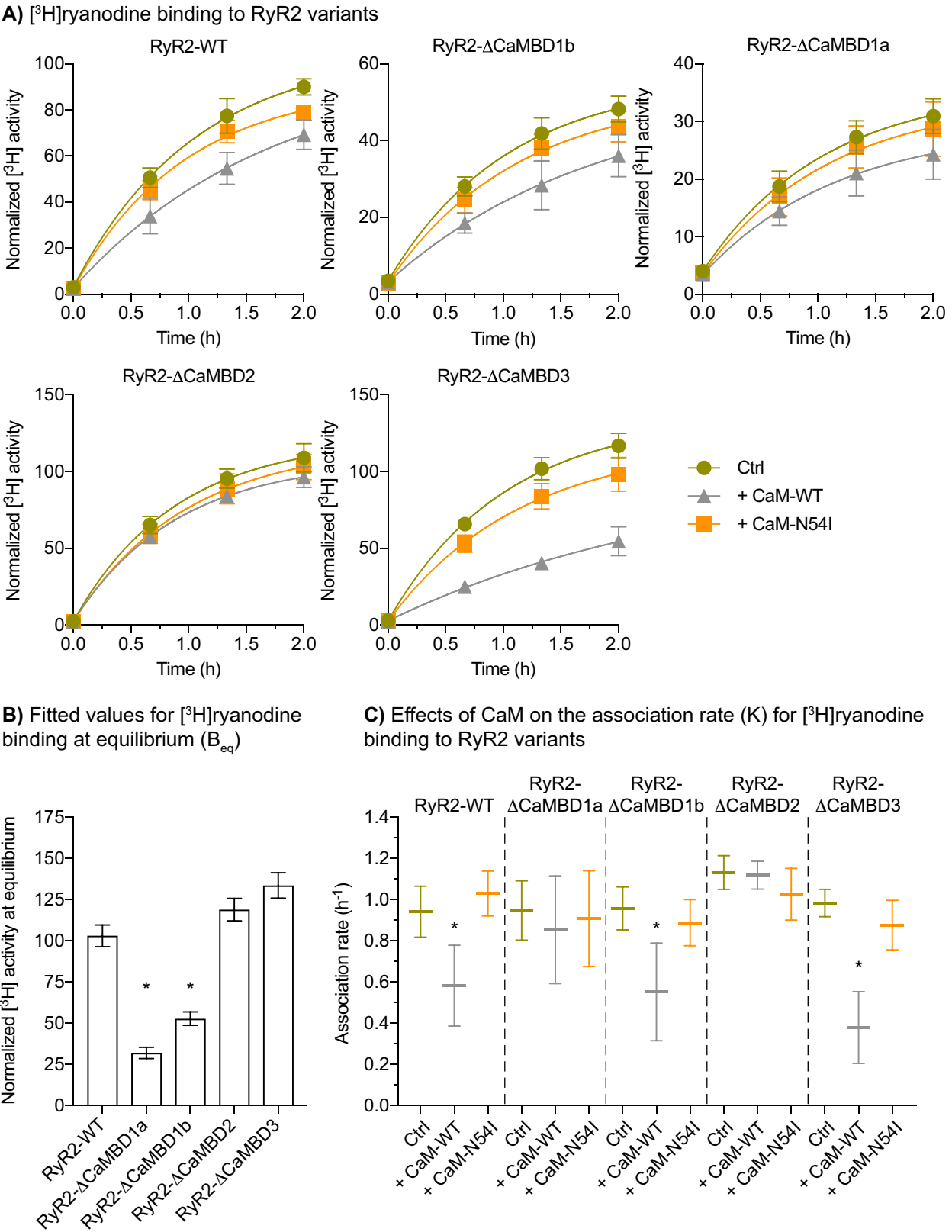
A) [3H]ryanodine binding to RyR2 variants
RyR2-WT
RyR2-ΔCaMBD1b
RyR2-ΔCaMBD1a
RyR2-ΔCaMBD2
RyR2-ΔCaMBD3
Normalized [3H] activity
Time (h)
Ctrl
+ CaM-WT
+ CaM-N54I
B) Fitted values for [3H]ryanodine binding at equilibrium (Beq)
Normalized [3H] activity at equilibrium
RyR2-WT
RyR2-ΔCaMBD1a
RyR2-ΔCaMBD1b
RyR2-ΔCaMBD2
RyR2-ΔCaMBD3
C) Effects of CaM on the association rate (K) for [3H]ryanodine binding to RyR2 variants
Association rate (h-1)
Ctrl
+ CaM-WT
+ CaM-N54I

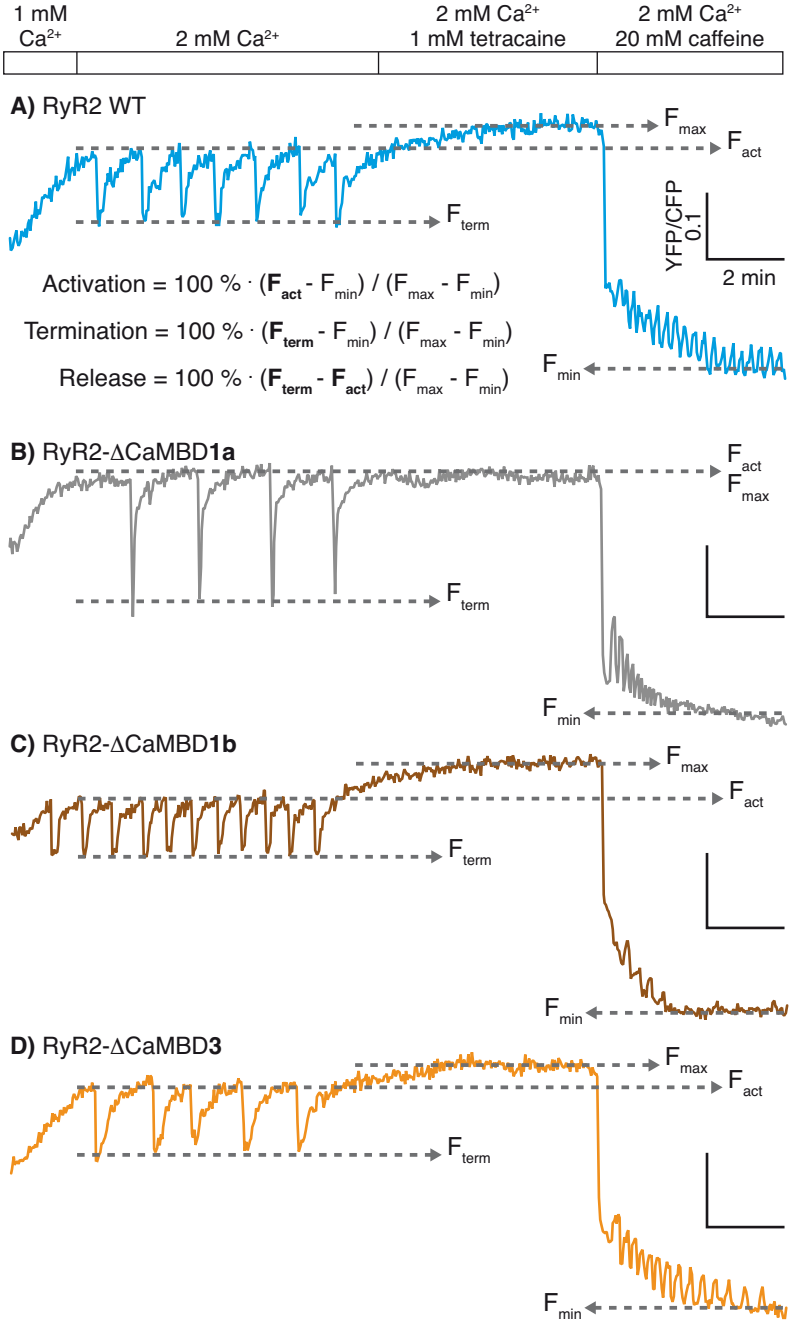
1 mM Ca2+
2 mM Ca2+
2 mM Ca2+ 1 mM tetracaine
2 mM Ca2+ 20 mM caffeine
A) RyR2 WT
Fmax
Fact
Fterm
Fmin
YFP/CFP 0.1
2 min
Activation = 100 % · (Fact - Fmin) / (Fmax - Fmin)
Termination = 100 % · (Fterm - Fmin) / (Fmax - Fmin)
Release = 100 % · (Fterm - Fact) / (Fmax - Fmin)
B) RyR2-ΔCaMBD1a
C) RyR2-ΔCaMBD1b
D) RyR2-ΔCaMBD3

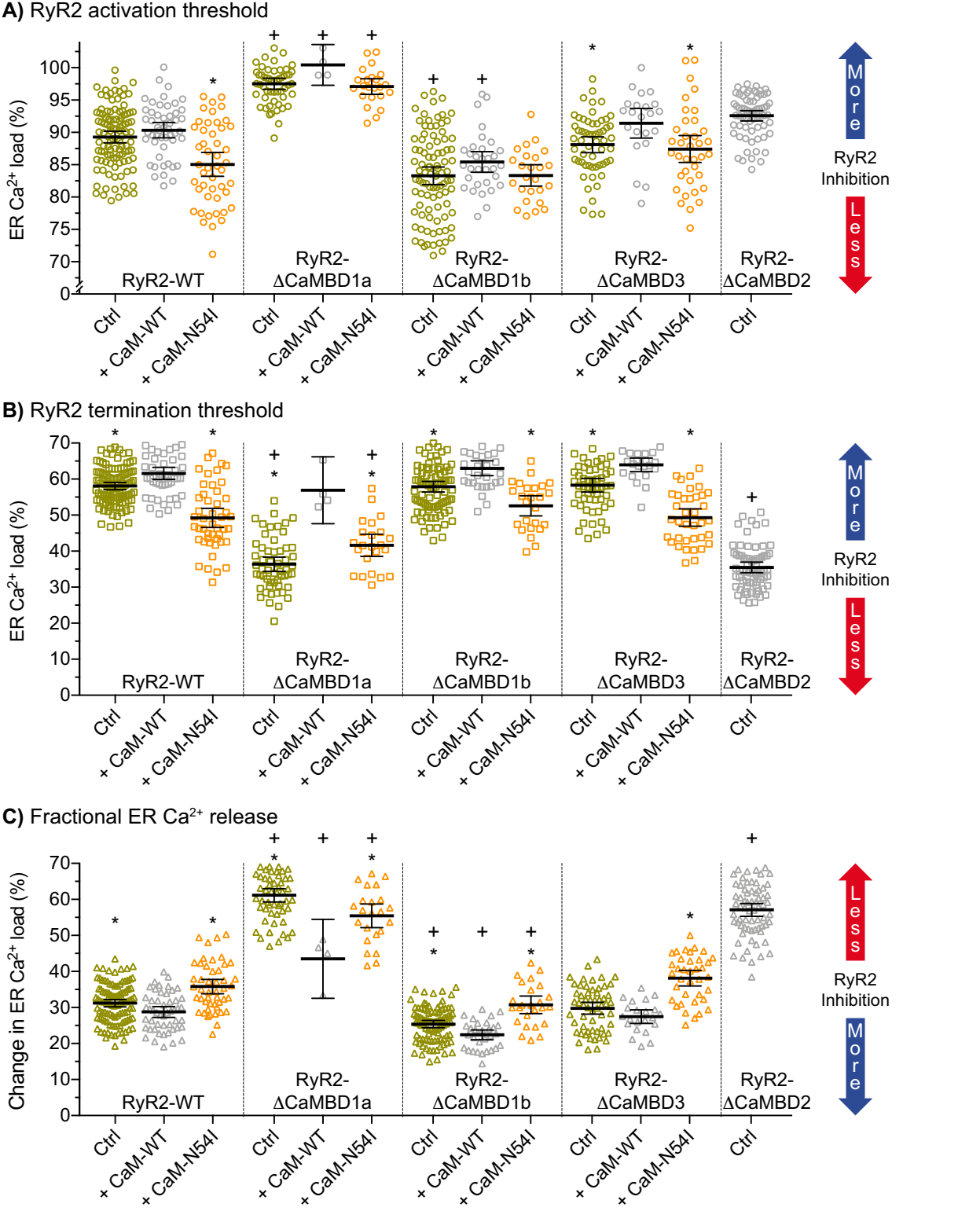
A) RyR2 activation threshold
ER Ca2+ load (%)
RyR2-WT
RyR2-ΔCaMBD1a
RyR2-ΔCaMBD1b
RyR2-ΔCaMBD3
RyR2-ΔCaMBD2
Ctrl
+ CaM-WT
+ CaM-N54I
More
RyR2 Inhibition
Less
B) RyR2 termination threshold
ER Ca2+ load (%)
RyR2-WT
RyR2-ΔCaMBD1a
RyR2-ΔCaMBD1b
RyR2-ΔCaMBD3
RyR2-ΔCaMBD2
Ctrl
+ CaM-WT
+ CaM-N54I
More
RyR2 Inhibition
Less
C) Fractional ER Ca2+ release
Change in ER Ca2+ load (%)
RyR2-WT
RyR2-ΔCaMBD1a
RyR2-ΔCaMBD1b
RyR2-ΔCaMBD3
RyR2-ΔCaMBD2
Ctrl
+ CaM-WT
+ CaM-N54I
Less
RyR2 Inhibition
More

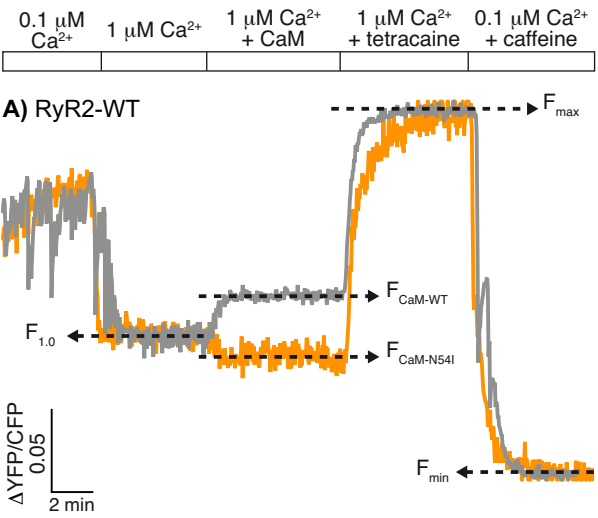

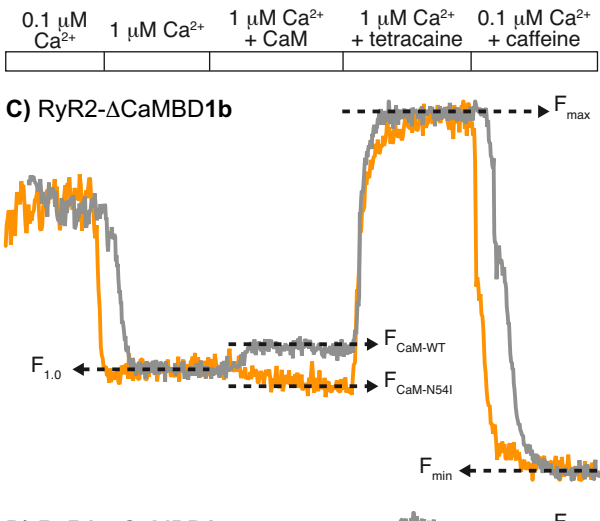

Without CaM = 100 % · ($\mathbf{F_{1.0}}$ - F_{min}) / (F_{max} - F_{min})

Effect of CaM-N54I = 100 % · ($\mathbf{F_{CaM\text{-}N54I}}$ - $\mathbf{F_{1.0}}$) / (F_{max} - F_{min})

Effect of CaM-WT = 100 % · ($\mathbf{F_{CaM\text{-}WT}}$ - $\mathbf{F_{1.0}}$) / (F_{max} - F_{min})

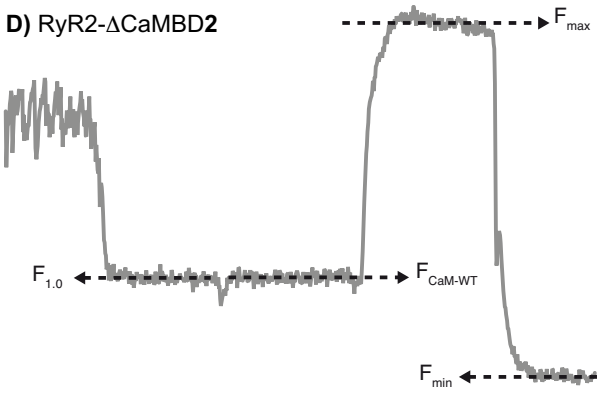

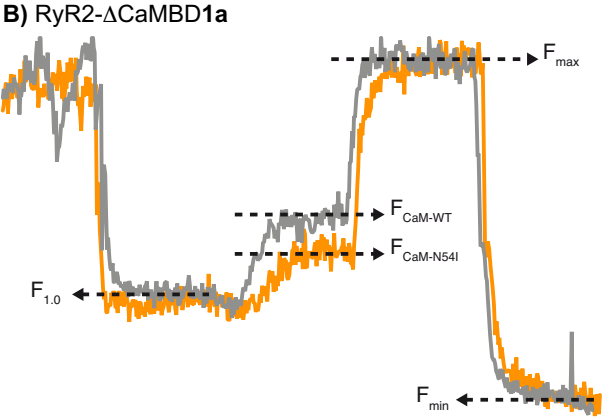

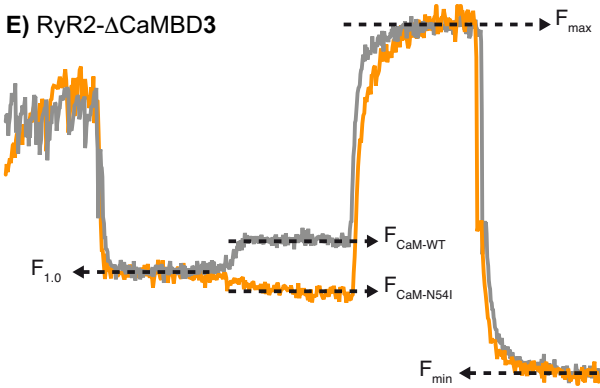

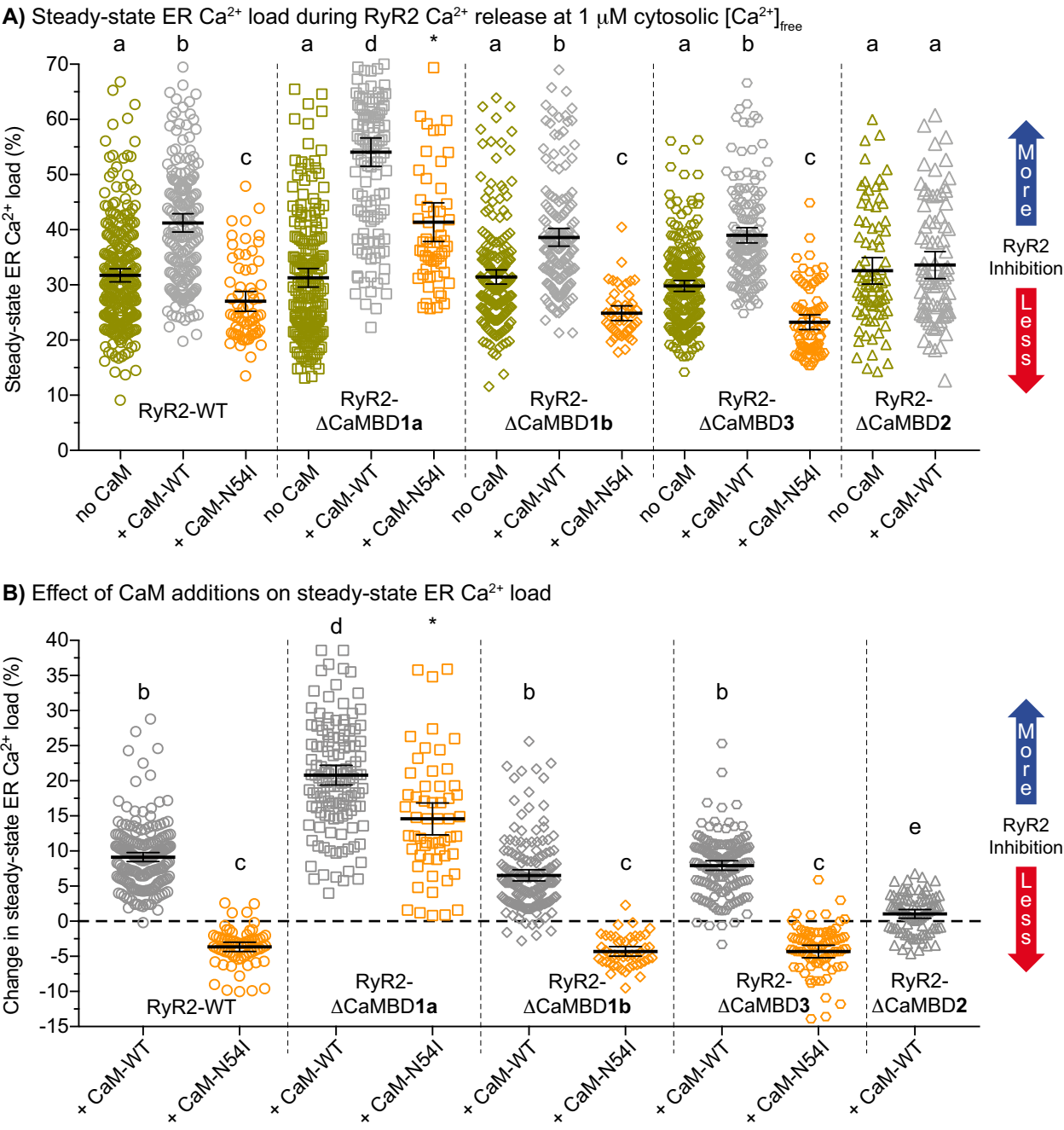
A) Steady-state ER Ca2+ load during RyR2 Ca2+ release at 1 μM cytosolic [Ca2+]free
Steady-state ER Ca2+ load (%)
a b a d * a b a b a a
c c c c
RyR2-WT
RyR2-ΔCaMBD1a
RyR2-ΔCaMBD1b
RyR2-ΔCaMBD3
RyR2-ΔCaMBD2
no CaM
+ CaM-WT
+ CaM-N54I
More RyR2 Inhibition Less
B) Effect of CaM additions on steady-state ER Ca2+ load
Change in steady-state ER Ca2+ load (%)
b d * b b b e
c c c c
RyR2-WT
RyR2-ΔCaMBD1a
RyR2-ΔCaMBD1b
RyR2-ΔCaMBD3
RyR2-ΔCaMBD2
+ CaM-WT
+ CaM-N54I
More RyR2 Inhibition Less

Figure 9

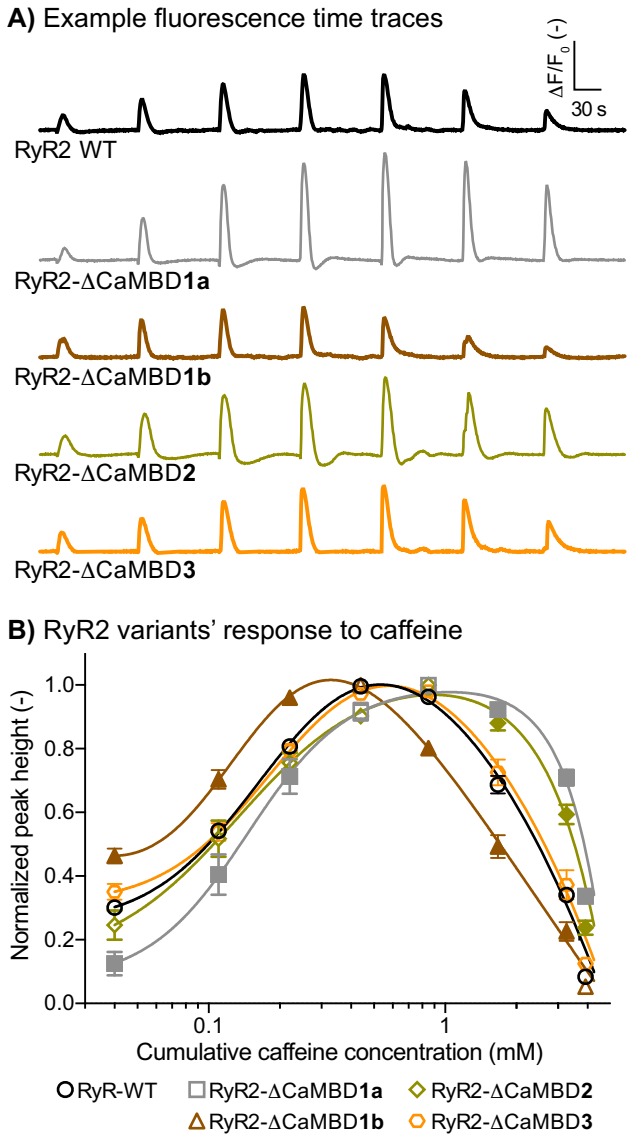
A) Example fluorescence time traces
ΔF/F0 (-)
30 s
RyR2 WT
RyR2-ΔCaMBD1a
RyR2-ΔCaMBD1b
RyR2-ΔCaMBD2
RyR2-ΔCaMBD3
B) RyR2 variants' response to caffeine
Normalized peak height (-)
1.0
0.8
0.6
0.4
0.2
0.0
0.1
1
Cumulative caffeine concentration (mM)
RyR-WT
RyR2-ΔCaMBD1a
RyR2-ΔCaMBD2
RyR2-ΔCaMBD1b
RyR2-ΔCaMBD3

A)

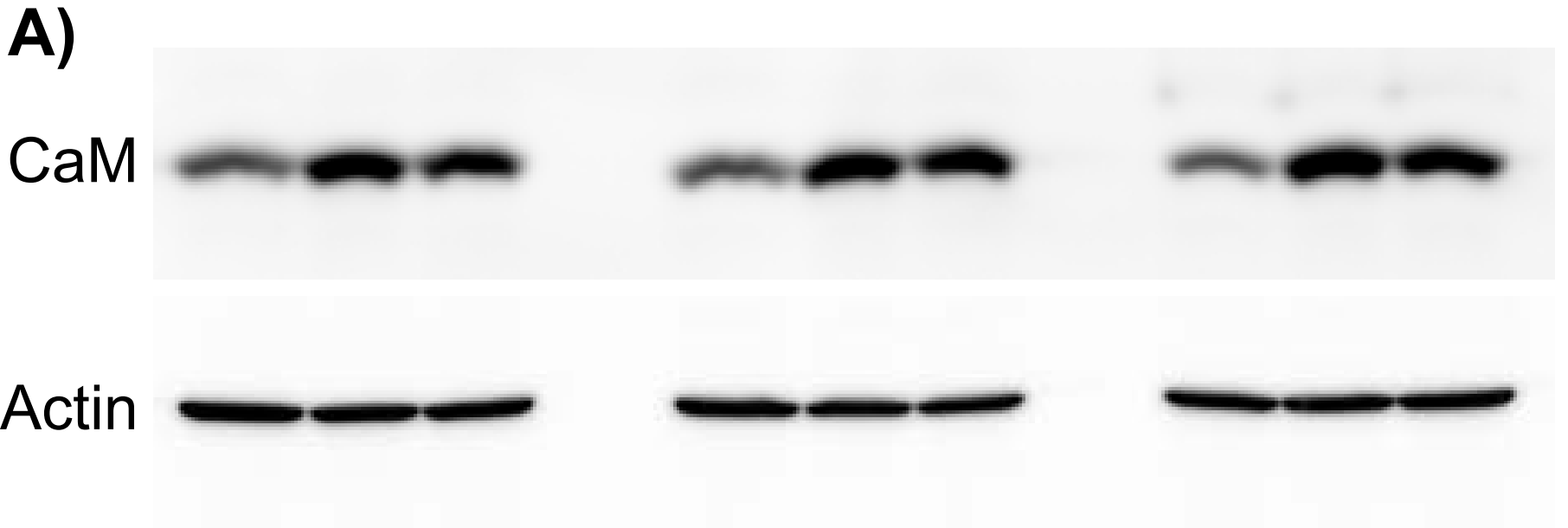
CaM
Actin

B)

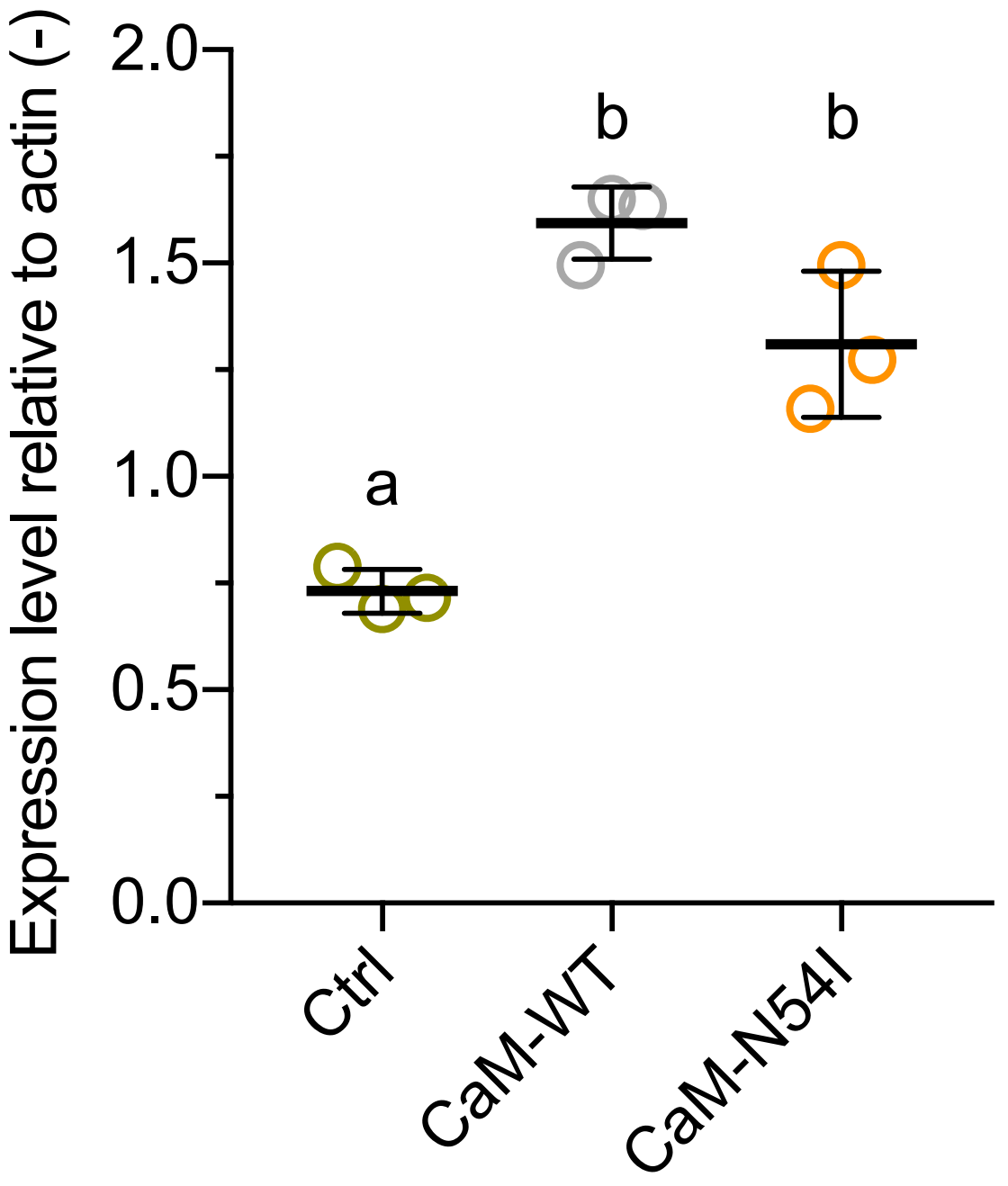
Expression level relative to actin (-)
2.0
1.5
1.0
0.5
0.0
a
b
b
Ctrl
CaM-WT
CaM-N54I